Supporting Information

Experimental Section……...2
Figure A1. ^{15}N NMR (THF-d_8, -75 ^{o}C) spectrum and simulation of **2**……...7
Figure A2. ^{1}H NMR (THF-d_8, -75 ^{o}C) spectrum of **2**……8
Figure A3. ^{1}H NMR spectra of **2** (22 ^{o}C) with various equiv of THF……...……9
Figure A4. ^{1}H NMR spectrum of **2** in C_6D_6 with 10 equiv hydrazine……...……...…10
Figure A5. ^{1}H{^{31}P} NMR spectrum of ^{15}N-enriched **3** (THF-d_8)……11
Figure A6. Simulation of the N*H* splitting in **3**……...…..11
Figure A7. Cyclic voltammetry of **3** in THF……...……12
Figure A8. UV-vis spectra of **3** and **4** in THF……...……...12
Figure A9. Overlaid rRaman spectra of **3** (^{14}N and ^{15}N)……...……...13
Figure A10. Overlaid rRaman spectra of **3** (^{14}N and ^{15}N)……...…..…14
Figure A11. Overlaid rRaman spectra of **4** (^{14}N and ^{15}N)……15
Figure A12. ^{1}H NMR spectrum of **4** (THF-d_8)……...……..16
Figure A13. EPR spectrum of **4** ……..……...……..16
Figure A14. Davies ^{15}N pulsed ENDOR spectra from ^{15}N-**4**, 2D field-frequency pattern……...17
Figure A15. Davies ^{15}N pulsed ENDOR spectra from ^{15}N-**4**, 2D field-frequency pattern…...…18
Figure A16. PESTRE spectra of ^{15}N-**4**……19
Figure A17. Isocontour plots (0.04) of the frontier orbitals of **3** and **4**……20
Figure A18. Isocontour plot (0.002) of the spin density of **4**……21
Table A1: Experimental and calculated bond distances and angles for **3** and **4**……...22
Figure A19. Displacement ellipsoid (50%) representation of **2**……23
Table A2. Select bond lengths [Å] and angles [°] for **2**……..24
Table A3. Crystal data and structure refinement for **2**……25
Figure A20. Displacement ellipsoid (50%) representation of **3**…….……...26
Table A4. Select bond lengths [Å] and angles [°] for **3**……..27
Table A5. Crystal data and structure refinement for **3**……28
Figure A21. Displacement ellipsoid (50%) representation of **4**……....29
Table A6. Bond lengths [Å] and angles [°] for **4**……....30
Table A7. Crystal data and structure refinement for **4**……31
Figure A22. Displacement ellipsoid (50%) representation of **[PhBP$_3$]Fe(CO)$_2$H**……..32
Table A8. Crystal data and structure refinement for **[PhBP$_3$]Fe(CO)$_2$H**. ……..33
Table A9. Bond lengths [A] and angles [deg] for **[PhBP$_3$]Fe(CO)$_2$H**. ……..34
References……..35

Experimental Section.

General Considerations. All manipulations were carried out using standard Schlenk, high-vac, or glove-box techniques under a dinitrogen atmosphere. Unless otherwise noted, solvents were deoxygenated and dried by sparging with Ar followed by passage through an activated alumina column from S.G. Water (Nashua, N.H.). Cyclopentane and 2-methyltetrahydrofuran were dried over sodium and benzophenone, and vac-transferred after the solution remained purple for 48 h. Non-halogenated solvents were tested with a standard purple solution of benzophenone ketyl in THF to confirm effective oxygen and moisture removal. Deuterated solvents were purchased from Cambridge Isotopes Laboratories, Inc. and were degassed and stored over activated 3-Å molecular sieves prior to use. Elemental analyses were performed Midwest Microlab (Indianapolis, IN).

Spectroscopic Measurements. Varian 300, 400, and 500 MHz spectrometers were used to record ^{1}H NMR, ^{31}P NMR, and ^{15}N NMR spectra (400 or 500 MHz). ^{1}H chemical shifts were referenced to residual solvent. ^{31}P NMR chemical shifts were referenced to 85% H_3PO_4 at $\delta = 0$ ppm, and ^{15}N NMR chemical shifts were referenced to neat $C_6H_5{}^{15}NO_2$ ($\delta = 370$ ppm) in comparison to liquid ammonia ($\delta = 0$ ppm). MestReNova (6.1.0) was used for NMR data workup, as well as for simulation of spectra.

IR measurements were obtained with a KBr solution cell or a KBr pellet using a Bio-Rad Excalibur FTS 3000 spectrometer controlled by Varian Resolutions Pro software set at 4 cm^{-1} resolution.

Room temperature rRaman samples were prepared by loading THF solutions into capillaries in the glove-box, which were then flame-sealed. Frozen solution samples were prepared by loading 2-MeTHF solutions into NMR tubes which were then flame-sealed. Excitation was performed at 632.8 nm using a HeNe laser (10 mW) or at 514 nm using an Ar ion laser. A lens collected the light that scattered at 90° and focused it through a low-pass filter and into the entrance slit of a SPEX 750M monochromator. The dispersed light was detected by a LN/CCD array (5 cm^{-1} resolution), and the spectra recorded using Winspec (Princeton Instrument) software. Conversion from pixels to wavenumber was done by obtaining the spectrum of cyclohexane, and deriving the linear plot of pixels versus wavenumber for known vibrations. All spectra were recorded in THF, and in some instances, solvent subtraction or baseline correction was performed.

Optical spectroscopy measurements were taken on a Cary 50 UV-Vis spectrophotometer using a 1 cm two-window quartz cell sealed with standard ground-glass joints or Teflon plugs.

Samples of **4** suitable for 35 GHz EPR and ENDOR measurements were prepared in 9:1 THF:2-MeTHF solvent mixtures (3 mM) and transferred into quartz tubes in the glovebox. The samples were frozen in the glovebox, and transferred/stored at 77K. EPR and ENDOR data were collected on a home-built spectrometer, described previously,[1] that was equipped with a liquid helium immersion dewar for measurements at 2 K. Echo-detected EPR spectra of ^{15}N-**4** were simulated using the Simfonia program.[2]

Signs of the hyperfine couplings measured from ENDOR spectra (more specifically, the sign of $g_{Nuc}A_{Nuc}$) have been obtained by application of the Pulse-Endor-SaTuration-REcovery

(PESTRE) protocol, a pulse sequence comprised of multiple Davies ENDOR sequences, carried out in three distinct experimental phases: (I) an EPR saturation phase (RF off) of 100 Davies sequences whose spin-echo intensities quickly converge to the steady-state 'baseline' (BSL); (II) an ENDOR perturbation phase of 24 sequences, in which each sequence contains a fixed RF set at one or the other of the branches of the ENDOR spectrum ($\nu_{\pm}$); (III) and an EPR recovery phase (RF off) of 132 sequences during which the spin echo corresponds to the spin-echo 'dynamic reference level' (*drl*) associated with ENDOR-induced spin polarization created in the second phase, with the *drl* relaxing to the BSL during this phase. In the slow-relaxation regime, the sign of A_{Nuc} is unambiguously given by the sign of the difference between the *drl* and BSL echo intensities as observed for *either* ENDOR branch.[3]

Under the typical conditions for a PESTRE experiment t_{mix}, defined as the time between the first and the second of the three microwave pulses within a single Davies sequence, is short relative to the electron spin-lattice relaxation time, T_{1e} ($T_{1e} >> t_{mix} \sim 5$ μs). However, for ^{15}N-**4**, in this regimethe PESTRE responses, namely the differences between the *drl* and BSL in phase III, re too small to make a reliable hyperfine sign assignment for both the nu+ and nu- manifolds. However, when t_{mix} is long and T_{1e} are of the same order of magnitude (t_{mix} = 5 ms in Figure A16) the difference between *drl* and BSL becomes readily measured. In this regime, the expected differences between the *drl* and BSL are of opposite sign to the short-t_{mix} experiment: for $\{A_n/g_n\} > 0$, if ν_+ is being interrogated, the *drl* relaxes to the BSL from *above*; if ν_- is interrogated, the *drl* relaxes to the BSL from *below*; the opposite behavior will be observed for $\{A_n/g_n\} < 0$.[4]

For ^{15}N-**4** in the long-t_{mix} regime, at ν_+ we observe the *drl* relaxing to the BSL from *below*; at ν_-, we observe the *drl* relaxing to the BSL from *above* (Figure A16), which implies that $\{A_n/g_n\} < 0$. As A_n is proportional to the product of gn and the spin density, the $\{A_n/g_n\}$ has the sign of the spin density. The experiment thus implies that the spin density on N is negative.

Electrochemistry. Electrochemical measurements were carried out in a glovebox under a dinitrogen atmosphere in a one-compartment cell using a BAS model 100/W electrochemical analyzer. A glassy carbon electrode and platinum wire were used as the working and auxiliary electrodes, respectively. The reference electrode was $Ag/AgNO_3$ in THF, and ferrocene was used as an internal standard. Solutions (THF) of electrolyte (0.4 M tetra-n-butylammonium hexafluorophosphate) and analyte were also prepared in a glovebox.

X-ray Crystallography Procedures. Low-temperature diffraction data were collected on a Siemens or Bruker Platform three-circle diffractometer coupled to a Bruker-AXS Smart Apex CCD detector with graphite-monochromated Mo or Cu Kα radiation (λ = 0.71073 or 1.54178 Å, respectively), performing φ-and ω-scans. The structures were solved by direct or Patterson methods using SHELXS[5] and refined against F^2 on all data by full-matrix least squares with SHELXL-97.[6] All non-hydrogen atoms were refined anisotropically. All hydrogen atoms (except hydrogen atoms on nitrogen) were included into the model at geometrically calculated positions and refined using a riding model. The isotropic displacement parameters of all hydrogen atoms were fixed to 1.2 times the U value of the atoms they are linked to (1.5 times for methyl groups). Hydrogen atoms directly coordinated to nitrogen were located in the Fourier difference map, and

refined semi-freely with the aid of distance restraints. If these hydrogen atoms could not be located in the difference map, they were left out of the final refinement model.

The structures were refined using established methods.[7] Several of the structures reported suffered from disorder in parts of the [$PhBP^{Ph}_3$] ligand and all of the structures showed disorder of solvent molecules (some over more than two independent positions). All disorders were refined with the help of similarity restraints on 1-2 and 1-3 distances and displacement parameters as well as rigid bond restraints for anisotropic displacement parameters. All close contacts, both inter and intramolecular, reported by the Platon validation software[8] involve at least one partner from a minor component of a disorder. While it is conceivable that more components of the molecule(s) are disordered and parameterization of these disordered components would remove the close contacts, the data at hand did not allow for further modeling of the disorder.

Crystals of **4** proved to be highly sensitive, with noticeable solvent loss/discoloration after ca. 1 minute in paratone oil. Their instability and small size did not allow us to collect a dataset using the above methods, and the dataset was collect at the Stanford Synchatron Radiation Laboratory (SSRL) beam line 12-2 at 17keV using a single phi axis and recorded on a Dectris Pilatus 6M. The ability to rotate just one-axis gave a dataset that was only 88.7% complete. The images were processed using XDS,[9] and XPREP was used to create appropriate files for use with the SHELXL-97 program.

The crystal structures have been deposited in the Cambridge Crystallographic Data Centre and have the following deposition numbers: CCDC 795818 – 795821.

DFT Calculations. Density functional calculations were carried out using the Gaussian03 suite[10] using the restricted B3LYP functional, unless otherwise noted. The 6-31+G* basis set was used to obtain a minimized structure of **3**, and the 6-311++G** basis set was used to do a single-point energy calculation from the optimized coordinates. The 6-31+G* basis set was used to obtain a minimized structure of **4** using the unrestricted BPV86 functional, and the 6-311++G** basis set was used to do a single-point energy calculation from the optimized coordinates (B3LYP).
For geometry optimizations, coordinates were taken from the solid-state structures of **3** and **4**. Truncation of the ligand by replacing the Ph substituents on the phosphines to Me groups gave a minimized structure in which the two carbonyl groups were *trans* to one another (~ C_{2h} symmetry), and hence all calculations were done with the full ligand, which preserved the observed coordination at both Fe centers. Molecular orbital plots were generated using GaussView 4.1[11] with isocontor values of 0.04 (MO) and 0.002 (density).

Starting Materials and Reagents. [$PhBP_3$]FeMe,[12] [$PhBP_3$]$Fe(CO)_2Na(THF)_6$,[13] and $^{15}N_2H_4$[14] were prepared according to literature methods. All other reagents were purchased from commercial vendors and used without further purification.

Synthesis of [$PhBP_3$]Fe(η^2-N_2H_3)(CO), 2.

1.) In the glovebox, a 20 mM THF solution of $[PhBP_3]FeMe$ (856.7 mg, 1.132 mmol) was transferred to a 500 mL round bottom flask, and stirred at -78 ^oC. To this, a solution of anhydrous hydrazine (55.0 μL, 1.699 mmol) in 5 mL THF was added dropwise. After stirring for 10 min, a calibrated bulb (56.30 mL) that was fit with Kontes Teflon plugs was attached to the flask, and the reaction taken out of the glovebox and quickly transferred to a dry ice/acetone bath. The bulb was attached to a high vacuum manifold and degassed. CO (1.132 mmol, 37.1 cmHg) was added to the bulb, which was then closed to the manifold, and opened to the reaction flask. The reaction was stirred for 18 h, during which time it gradually warmed to room temperature. The volatiles were removed, and in the glovebox, the solids were rinsed with 20 mL of pentane. The solids were then extracted into minimum THF, filtered, and layered with an equal volume of pentane and stored at -35 ^oC. As $[PhBP_3]Fe(CO)_2H$ readily co-crystallizes with **2**, crystals of analytically pure **2** are only obtained after several re-crystallizations (yield: 36.1 mg, 4.0 %). Synthetically useful samples of **2** can be obtained in yields that range between 30 – 40 %. Crystals of **2** suitable for diffraction can be grown by slow evaporation of pentane into a saturated benzene solution of **2** that contains hydrazine.

2.) A 25 mL schlenk tube fitted with a 8mm Kontes Teflon plug was charged with a stir bar and a 25 mM solution of $[PhBP_3]FeMe$ (31.9 mg, 0.0423 mmol) in THF. The flask was cooled to -78 ^oC using a dry ice/acetone bath. To this, a solution of anhydrous hydrazine (2.1 μL, 0.0633 mmol) in 0.4 mL THF was added dropwise, and a color change from amber to strawberry red was noted. The flask was sealed, removed from the glovebox, and immediately placed in a dry ice/acetone bath. The flask was connected to a calibrated bulb (3.24 mL) which was attached to a high vacuum manifold. Once full vacuum was attained (5.1 x 10^{-4} torr), the flask was degassed and closed to the vacuum manifold. CO (0.0423 mmol, 24.0 cmHg) was added to the caliberated bulb, which was then closed to the vacuum manifold and opened to the reaction flask. The reaction was stirred, and allowed to gradually warm to room temperature over the course of 14 h. At this time, the volatiles were removed to yield an orange solid. The solid was taken up in C_6D_6, and ^{31}P NMR data was collected, indicating 68 % conversion to **2**, with 18% conversion to $\{[PhBP_3]Fe\}_2(\mu\text{-}\eta^2\text{:}\eta^2\text{-}N_2H_2)(\mu\text{-}\eta^1\text{:}\eta^1\text{-}N_2H_4)$ and 10 % conversion to $[PhBP_3]Fe(CO)_2H$ (integration against an internal standard of PPh_3).

^1H NMR (THF-d_8, 500 MHz, -75 ^oC): δ 6.2-8.0 (m, 36H), 2.84 (s, 1H), 1.87 (s, 1H), 1.39 (bs, 4H), 0.95-1.20 (m, 2H). ^{31}P NMR (THF-d_8, 202 MHz, -75 ^oC): δ 64.23 (d, J = 82.6 Hz), 58.99 (d, J = 55.5 Hz), 32.59 (dd, J = 82.3, 55.4 Hz). IR (KBr) (cm^{-1}): 3316, 3237, 1917 (CO). UV-vis (THF) λ_{max}, nm (ε, M^{-1} cm^{-1}): 365 (sh, 1580), 492 (sh, 190), 720 (130). Anal. Calcd. for $C_{46}H_{44}BFeP_3N_2O$: C 69.02; H 5.54; N 3.50. Found: C 68.69; H 5.65; N 3.56.

A sample of 95% ^{15}N-enriched **2** was synthesized using an analogous synthetic procedure with $^{15}NH_2{}^{15}NH_2$. ^1H NMR (THF-d_8, 500 MHz, -75 ^oC): δ 6.45 (d, N*H*H, $^1J_{NH}$ = - 86 Hz, 1H), 2.88 (d, NH*H*, $^1J_{NH}$ = - 79 Hz, 1H), 1.88 (d, N*H*, $^1J_{NH}$ = - 56 Hz, 1H). Select $^1H\{^{31}P\}$ decoupling indicates that the peak at 6.45 ppm is coupled to the ^{31}P NMR resonance at 32.59, suggesting that this proton resonance corresponds to the $NH\mathit{H}_{trans}$ to the phosphine. ^{15}N NMR (THF-d_8, 50 MHz, -75 ^oC): δ 32.2 (m, *N*H, $^1J_{NH}$ = - 86 Hz, $^1J_{NN}$ = 10 Hz), 31.8 (m, *N*H_2, $^1J_{NH}$ = - 79 Hz, $^1J_{NH}$ = - 86

Hz, $^1J_{NN}$ = 10 Hz). Coupling constants were obtained by simulation of the spectrum. IR (KBr) (cm^{-1}): 3300, 3250, 3226.

Synthesis of {[PhBP$_3$]Fe(CO)}$_2$(μ-η^1:η^1-*trans*-N$_2$H$_2$), 3. Complex **2** (0.0224 g, 0.0280 mmol) was taken up in 1 mL C_6D_6 and transferred to a J.Young tube. The tube was attached to a calibrated bulb (3.24 mL) on a high vacuum manifold. The solution was frozen and evacuated. Oxygen (0.0140 mmol, 8.0 cmHg) was added to the bulb, which was then closed to the manifold. The oxygen was condensed into the tube (liquid nitrogen), and sealed. The reaction was thawed, and shaken once. After 18 h, the solution had changed color from orange to blue-green. The NMR tube was rotated for an addition 6 h, during which the color changed to blue. In the glovebox, the volatiles were removed, and the solid residue was washed with pentane and diethyl ether, to afford **3** as an analytically pure blue solid (yield: 0.0136 g, 61.9%). Crystals suitable for diffraction could be grown by diffusion of pentane into a benzene solution of **3**. $^1H\{^{31}P\}$ NMR (400 MHz, THF-d_8) δ 9.5 (bs, 2H, N*H*), 7.72 (d, *J* = 7.4 Hz, 4H), 7.67 (d, *J* = 6.4 Hz, CH_{ortho} 8H), 7.24 (t, *J* = 7.5 Hz, 8H), 6.9-7.15 (m, 50 H), 1.89 (s, CH_2, 4H), 1.53 (d, *J* = 13.4 Hz,C*H*H, 4H), 1.20 (d, *J* = 14.4 Hz, CH*H*, 4H). ^{31}P NMR (162 MHz, THF-d_8) δ 57.04 (d, *J* = 55.3 Hz), 38.95 (t, *J* = 55.6 Hz). IR (THF/KBr) (cm^{-1}): 3270 (NH), 569. IR (KBr) (cm^{-1}): 1931 (CO). rRaman (633 nm) (cm^{-1}): 1060 (NN), 665 (FeN). UV-vis (THF) λ_{max}, nm (ε, M^{-1} cm^{-1}): 527 (sh, 2650), 716 (8470). Anal. Calcd. for $C_{92}H_{84}B_2Fe_2P_6N_2O_2$: C 70.43; H 5.40; N 1.78. Found: C 71.08; H 6.34; N 1.57.

A sample of 95% ^{15}N-enriched **3** was synthesized using an analogous synthetic procedure with ^{15}N-enriched **2**. $^1H\{^{31}P\}$ NMR (400 MHz, THF-d_8) δ 9.495 (m, $^1J_{NH}$ = -71.0 Hz, $^2J_{NH}$ = -2.1 Hz, $^3J_{HH}$ = 14.8 Hz, $^1J_{NN}$ = -9.5 Hz, 2H, N*H*). Coupling constants were obtained by simulation of the spectrum. ^{15}N NMR (THF-d_8, 40 MHz): δ 291.9 (d, *J* ≈ 71 Hz). IR (THF/KBr) (cm^{-1}): 3264 (NH), 565. rRaman (633 nm) (cm^{-1}): 1030 (NN), 651 (FeN).

Synthesis of {[PhBP$_3$]Fe(CO)}$_2$(μ-η^1:η^1-*trans*-N$_2$H$_2$).Na(THF)$_6$, 4. A solution of **3** (3.7 mg, 0.0024 mmol) in 2 mL THF was added to a stirring 0.32 wt % Na/Hg amalgam (16.9 mg, 0.0024 mmol). After an hour, the reaction solution changed color from blue to purple. The reaction was filtered, and the volatiles were removed to give pure **4** (4.4 mg, 92 %). Crystals suitable for x-ray diffraction were grown by slow diffusion of cyclopentane into a saturated THF solution of **4**. ^1H NMR (300 MHz, THF-d_8) δ 8.3 (bs), 7.51, 7.18, 6.86. 4.73, 3.64 (coordinated THF), 1.78 (coordinated THF), 1.23, 0.89. UV-vis (THF) λ_{max}, nm (ε, M^{-1} cm^{-1}): 532 (5000), 630 (3690). rRaman (633 nm) (cm^{-1}): 643 (FeN). EPR (35 GHz, 2K, 9:1 THF:2MeTHF): g = [2.125, 2.040, 2.020]. Anal. Calcd. for $C_{116}H_{132}B_2Fe_2P_6N_2O_8Na$: C 68.82; H 6.57; N 1.38. Found: C 62.55; H 5.71; N 2.04.

A sample of 95% ^{15}N-enriched **4** was synthesized using an analogous synthetic procedure with ^{15}N-enriched **3**. rRaman (633 nm) (cm^{-1}): 624 (FeN).

Independent Synthesis of [PhBP$_3$]Fe(CO)$_2$H. A solution of triflic acid (10.8 μL, 0.123 mmol) in 2 mL THF was added dropwise to a stirring solution of [PhBP$_3$]Fe(CO)$_2$Na(THF)$_6$ (0.1450 g, 0.1225 mmol) in 10 mL THF. After 10 min, the solution changed color from bright orange to pale yellow, and the volatiles were removed. The resulting solid was rinsed with pentane, extracted into benzene and filtered through celite. Layering the benzene solution with pentane

gave crystals suitable for diffraction (0.0779 g, 98 %). ^{1}H NMR (300 MHz, C_6D_6) δ 7.99 (d, J = 7.1 Hz, 2H), 7.54-7.66 (m, 12H), 7.36 (t, J = 7.2 Hz, 1H), 6.66-6.86 (m, 20H), 1.76 (d, 2H, J_{PH} = 13.0 Hz), 1.66 (bs, 4H), -9.42 (td, J = 42.1, 21.2 Hz, 1H). ^{31}P NMR (121 MHz, C_6D_6) δ 47.55 (dd, J = 41.0, 9.8 Hz, 2P), 37.66 (t, J = 41.6 Hz, 1P). IR (KBr) (cm^{-1}): 2004, 1914 (CO). Anal. Calcd. for $C_{47}H_{42}BFeP_3O_2$: C 70.70; H 5.30; N 0. Found: C 70.65; H 5.67; N 0.

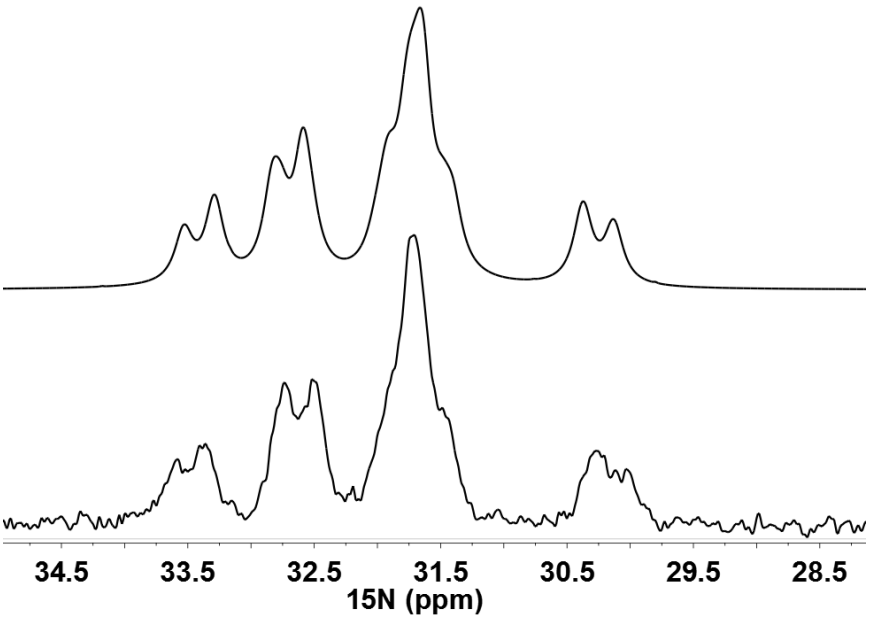

Figure A1. Simulation (top) of the ^{15}N NMR spectrum of **2** (-75 ^{o}C, [D_8]THF) and experimental spectrum (bottom). Pertinent fitting parameters: δ 31.8 (NH*N*H_2, ^{1}J(N,H) = 86 Hz, ^{1}J(N,H) = 79 Hz, ^{1}J(N,N) = 10 Hz), 32.2 (*N*HNH_2, ^{1}J(N,H) = 56 Hz), linewidth = 7 Hz.

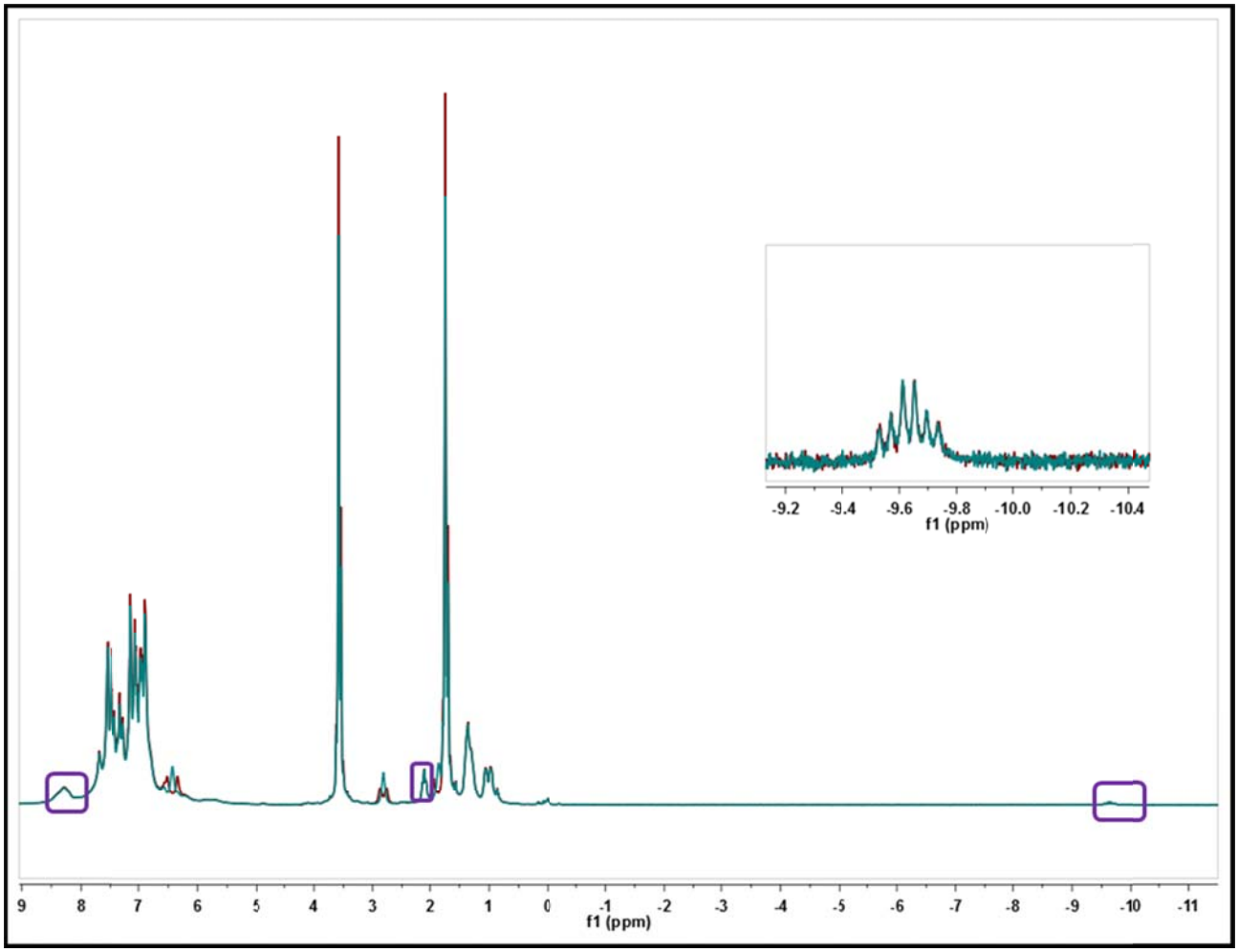

Figure A2. Overlay of ^{1}H (red) and $^{1}H\{^{31}P\}$ (blue) NMR (THF-d_8, -75 ^{o}C) spectrum of **2** prepared with $^{15}N_2H_4$. Peaks marked by a purple box are due to $[PhBP_3]Fe(CO)_2H$, with the inset indicating the hydride resonance of $[PhBP_3]Fe(CO)_2H$.

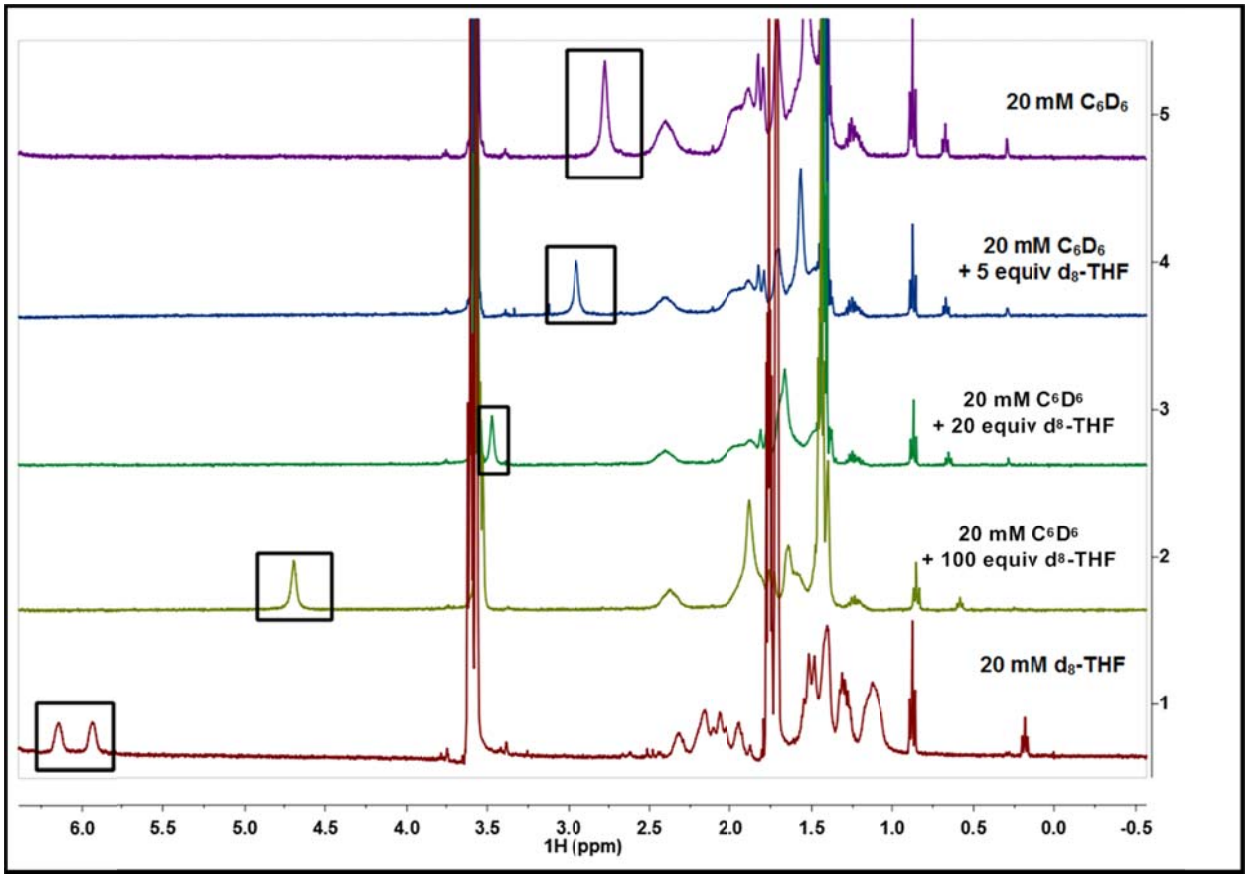

Figure A3. ^{1}H NMR spectra of **2** (22 ^{o}C) in various solvent ratios. The spectrum in THF-d_8 is ^{15}N-enriched. The NHH_{trans} resonance is shown in a black box, highlighting the effect of hydrogen-bonding to THF.

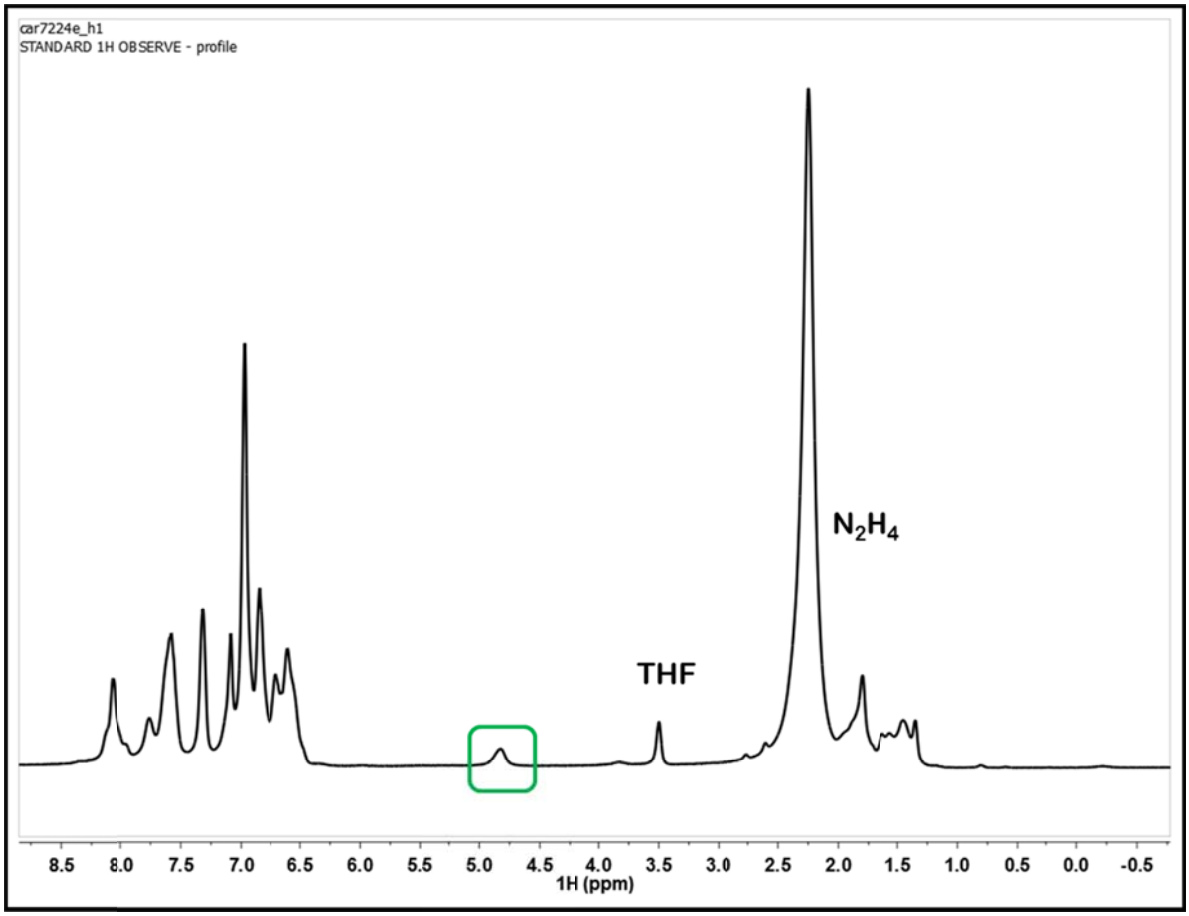

Figure A4. ^{1}H NMR spectrum of **2** in C_6D_6 with the addition of 10 equiv of N_2H_4. The resonance that corresponds to NHH_{trans} is indicated in the green box, and is shifted from 2.78 ppm (in C_6D_6) to 4.78 ppm, due to hydrogen bonding.

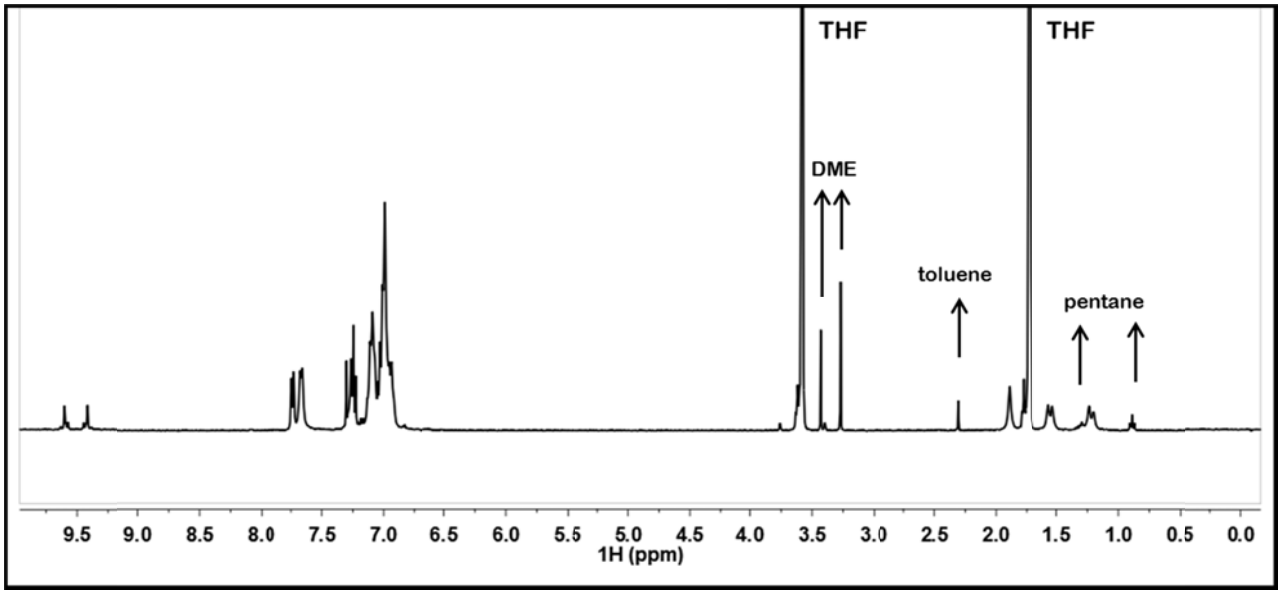

Figure A5. $^{1}H\{^{31}P\}$ NMR spectrum of ^{15}N-enriched **3** (THF-d_8).

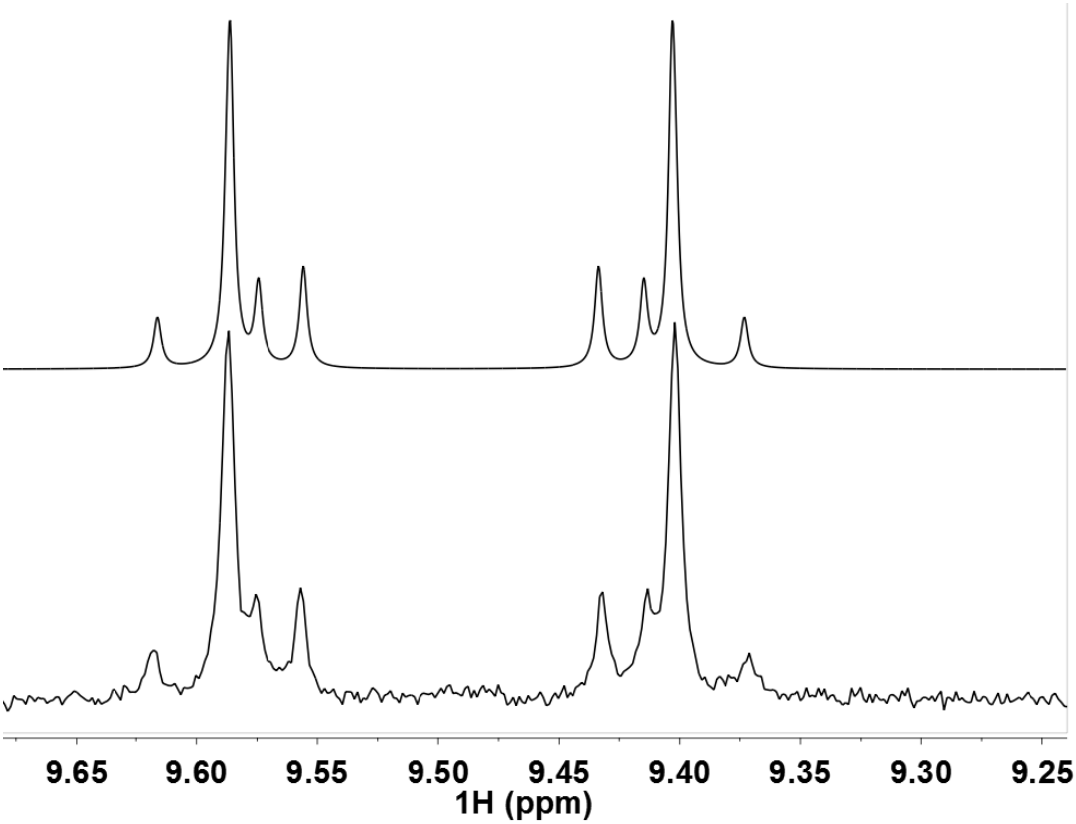

Figure A6. Simulation (top) and experimental (bottom) ^{1}H NMR spectrum of the N*H* proton in ^{15}N-enriched **3**. Fitting parameters: δ 9.494, $^{1}J_{NH}$ = -71.0 Hz, $^{2}J_{NH}$ = -2.1 Hz, $^{3}J_{HH}$ = 14.8 Hz, $^{1}J_{NN}$ = 9.5 Hz.

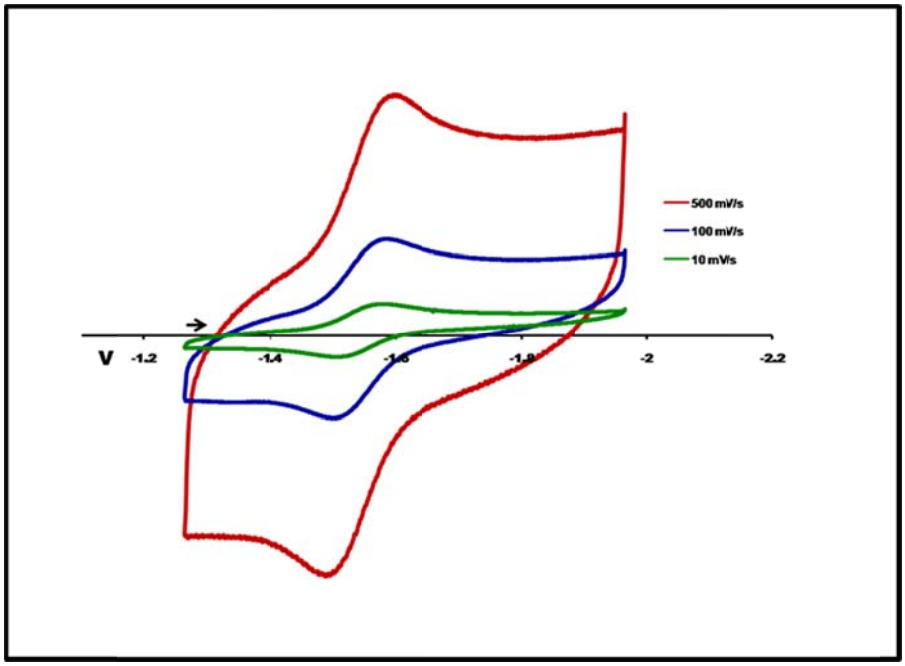

Figure A7. Cyclic voltammogram of **3** in THF. Experimental parameters: 0.45 mM analyte, 0.4 M TBA.PF_6, scan rate as noted.

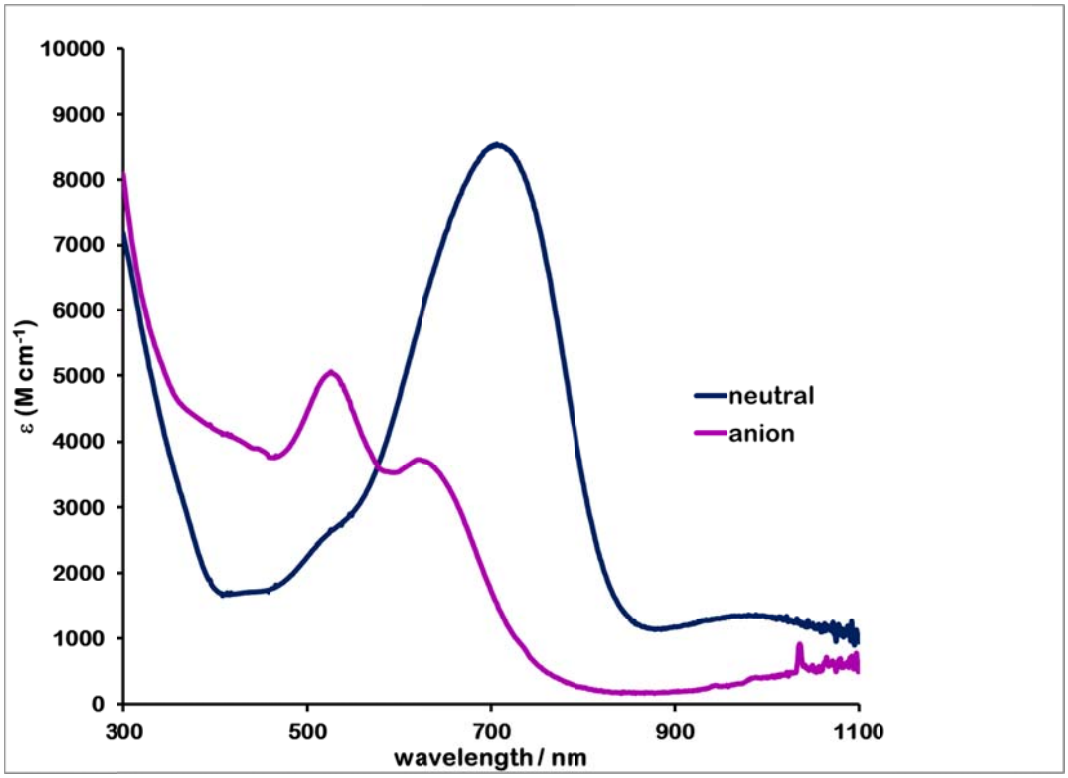

Figure A8. UV-vis spectra of **3** and **4** in THF.

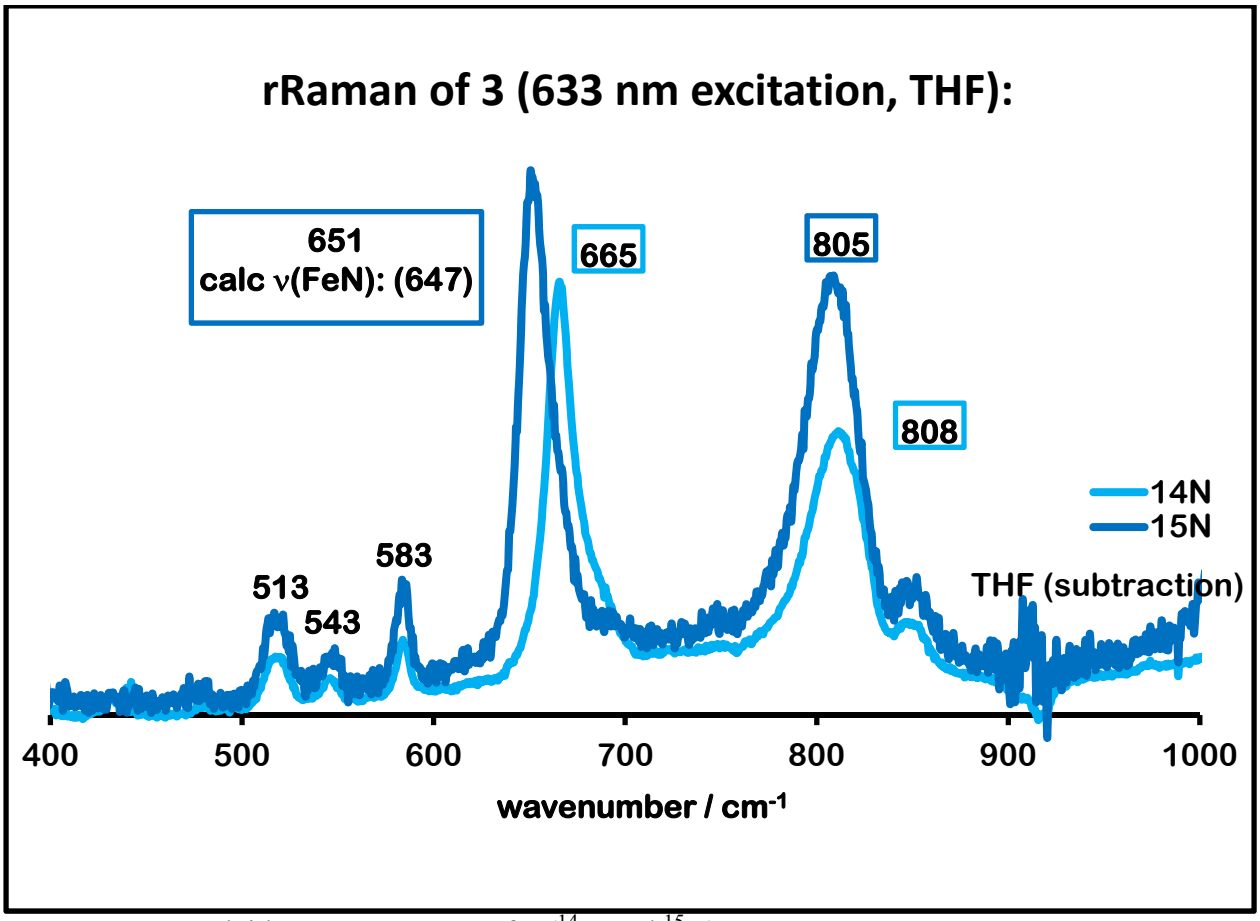

Figure A9. Overlaid rRaman spectra of **3** (^{14}N and ^{15}N).

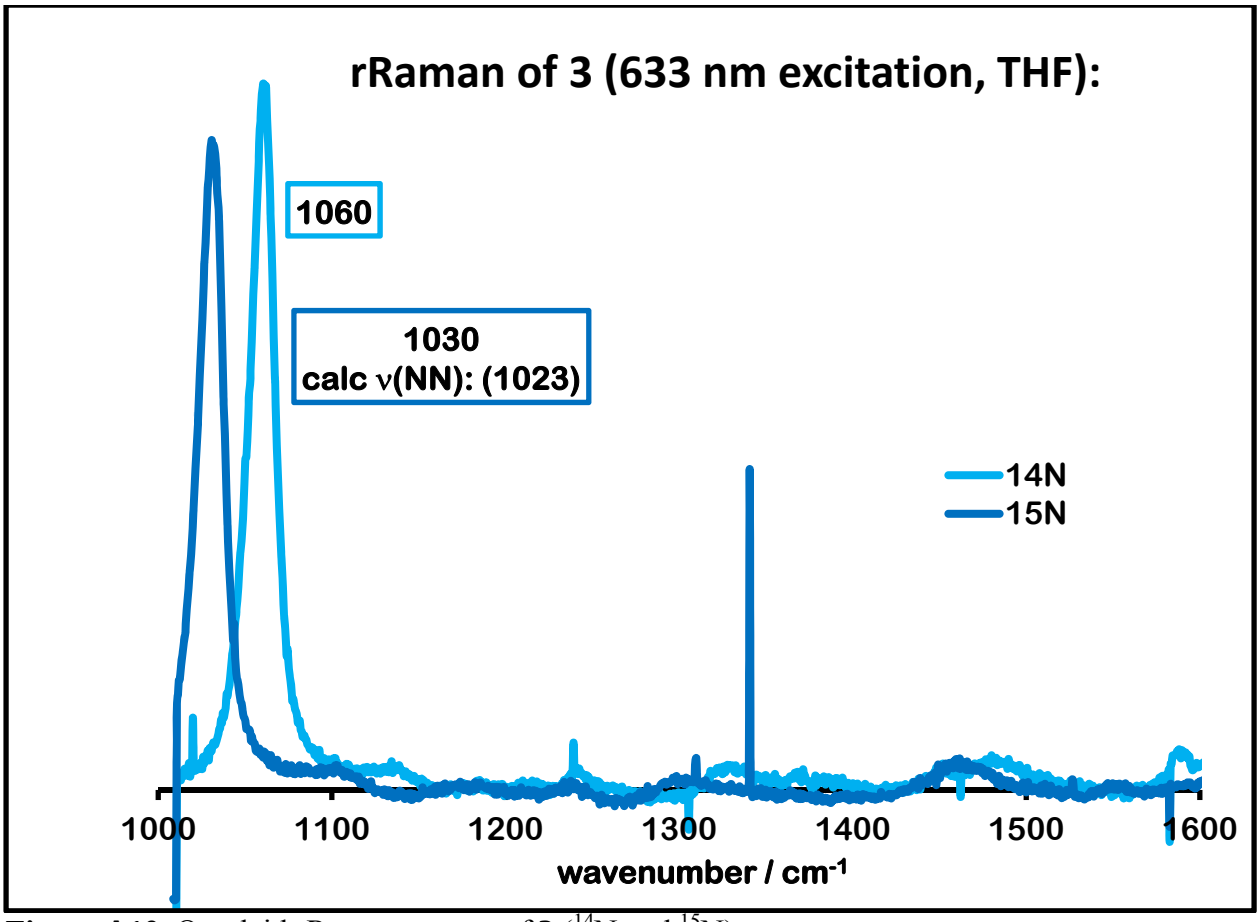

Figure A10. Overlaid rRaman spectra of **3** (^{14}N and ^{15}N).

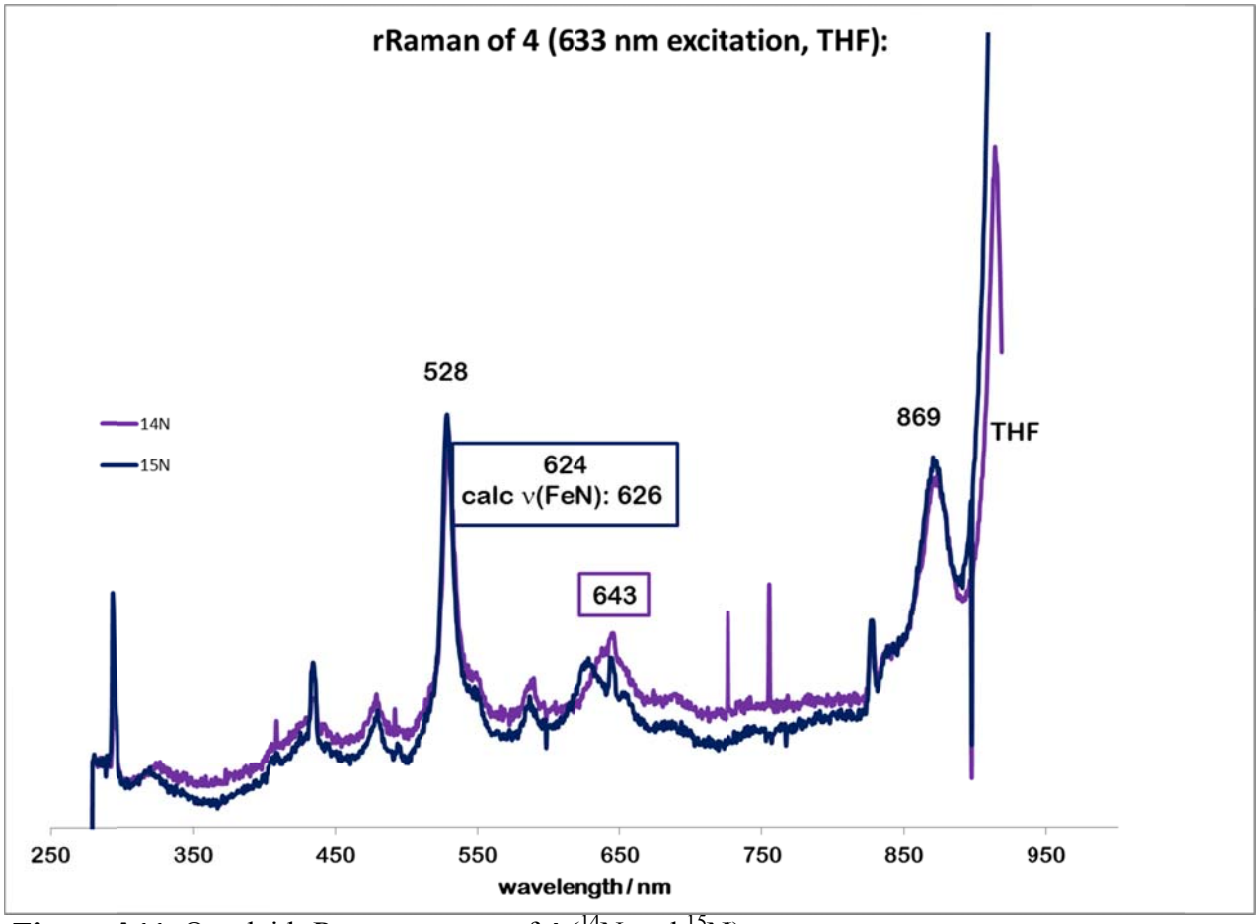

Figure A11. Overlaid rRaman spectra of **4** (^{14}N and ^{15}N).

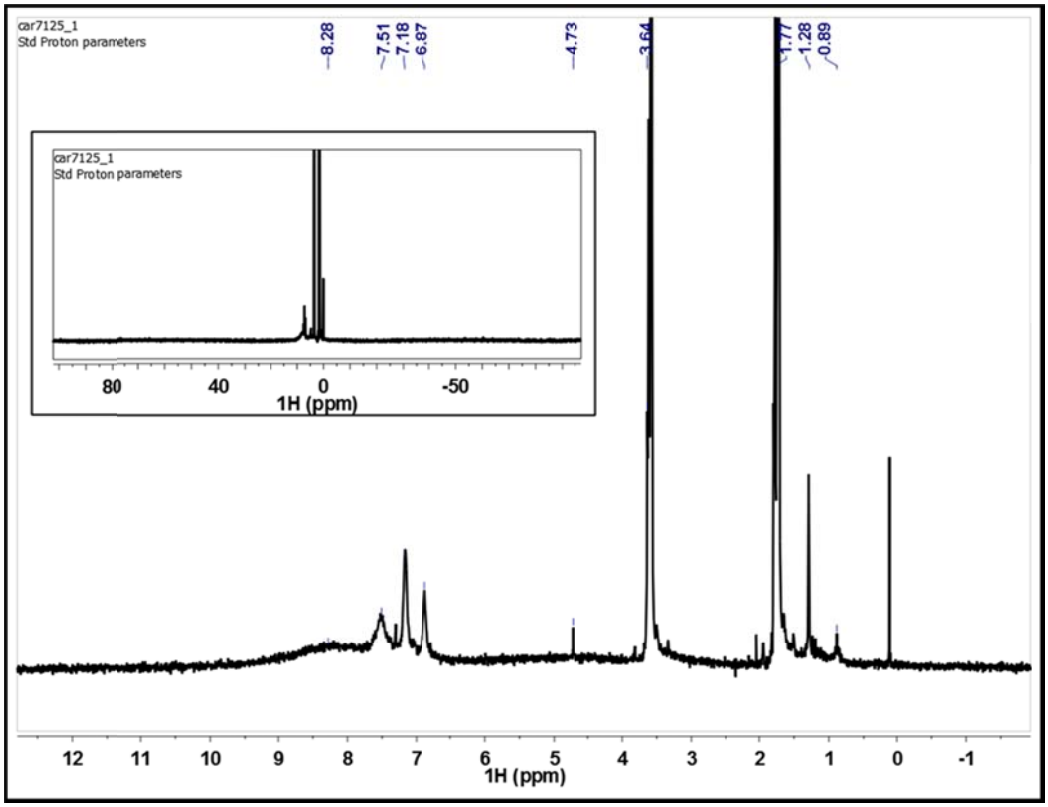

Figure A12. ^{1}H NMR spectrum of **4** (THF-d_8). The inset shows the same spectrum in a larger chemical shift window.

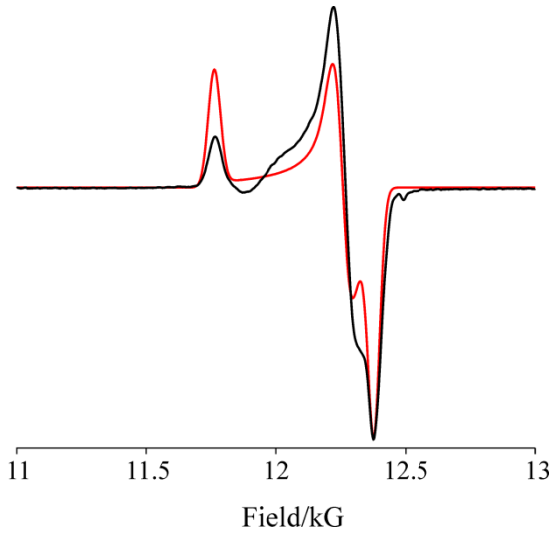

Figure A13. Two-pulse echo-detected EPR spectrum of **4** (red) and fit (black). *Experimental Conditions*: pulse length, π = 200 ns; microwave frequency, 35.003 GHz, repetition time, 20 ms; τ = 600 ns; 20 shots per point, temperature, 2 K. Spectrum was simulated with g = [2.125, 2.040, 2.120], and an anisotropic Gaussian linewidth of [55, 65, 45] G to account for the EPR linewidth contribution that is due to unresolved hyperfine couplings.

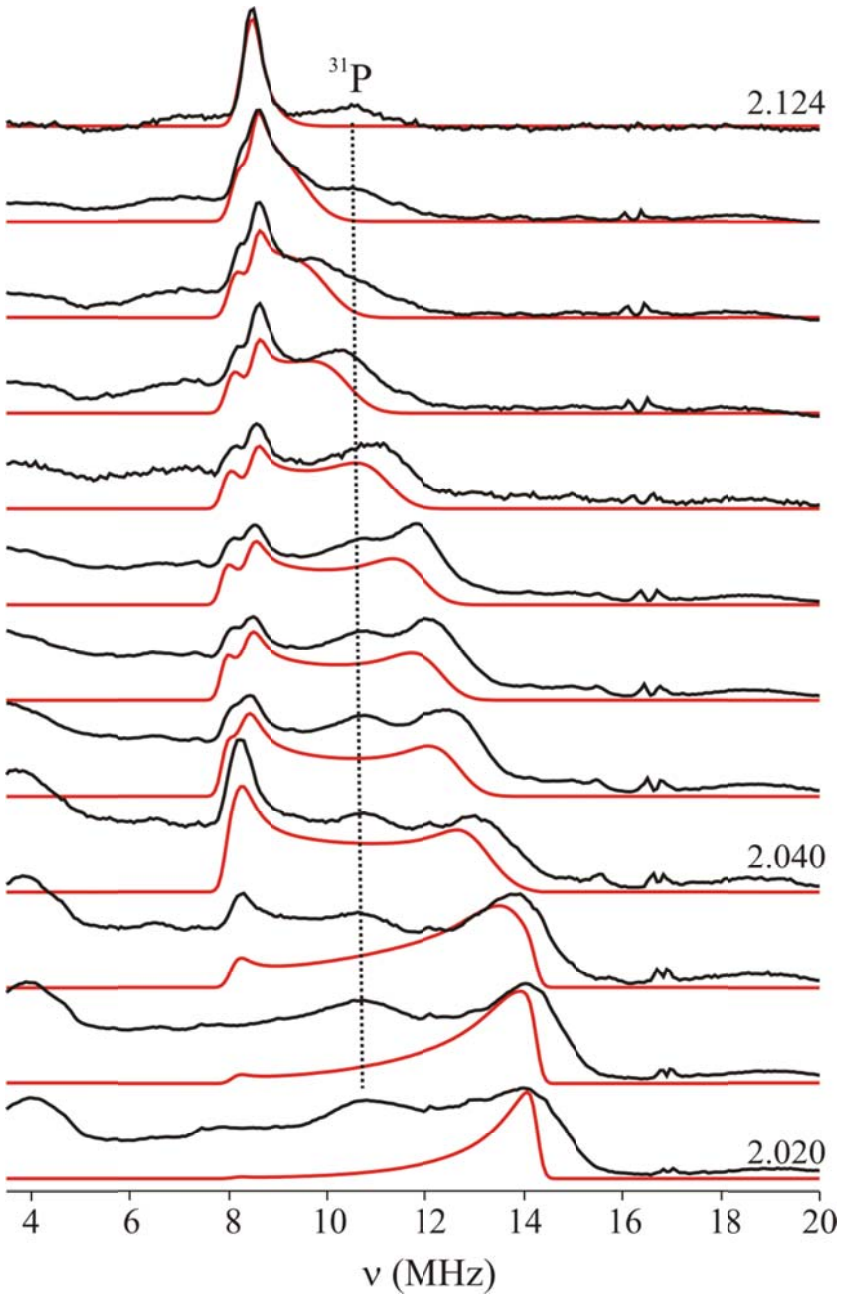

Figure A14. Davies ^{15}N pulsed ENDOR spectra from ^{15}N-**4**, 2D field-frequency pattern (black traces) with simulations (red traces). The spectra have been simulated using a single type of ^{15}N nucleus whose hyperfine tensor is rotated relative to **g** by $\alpha = 7^{o}$ around the N-N vector (g_1). The dotted black line corresponds to an ENDOR response from ^{31}P nuclei in **4**. *Experimental conditions*: microwave frequency, 34.922-34.983 GHz; π = 200 ns; τ = 600 ns; t_{rf} = 30 μs; repetition rate, 20 ms; RF randomly hopped. *Simulations*. g = [2.125, 2.040, 2.020] (g_1 = z); A = [6.7, 5.3, 17.8] MHz; (φ,θ,ψ) = (90,25,90 + α); microwave frequency, 34.983 GHz; EPR linewidth, 300 MHz; ENDOR linewidth, 0.25 MHz; the maximum simulation intensity is individually matched to the maximum ENDOR intensity at each field.

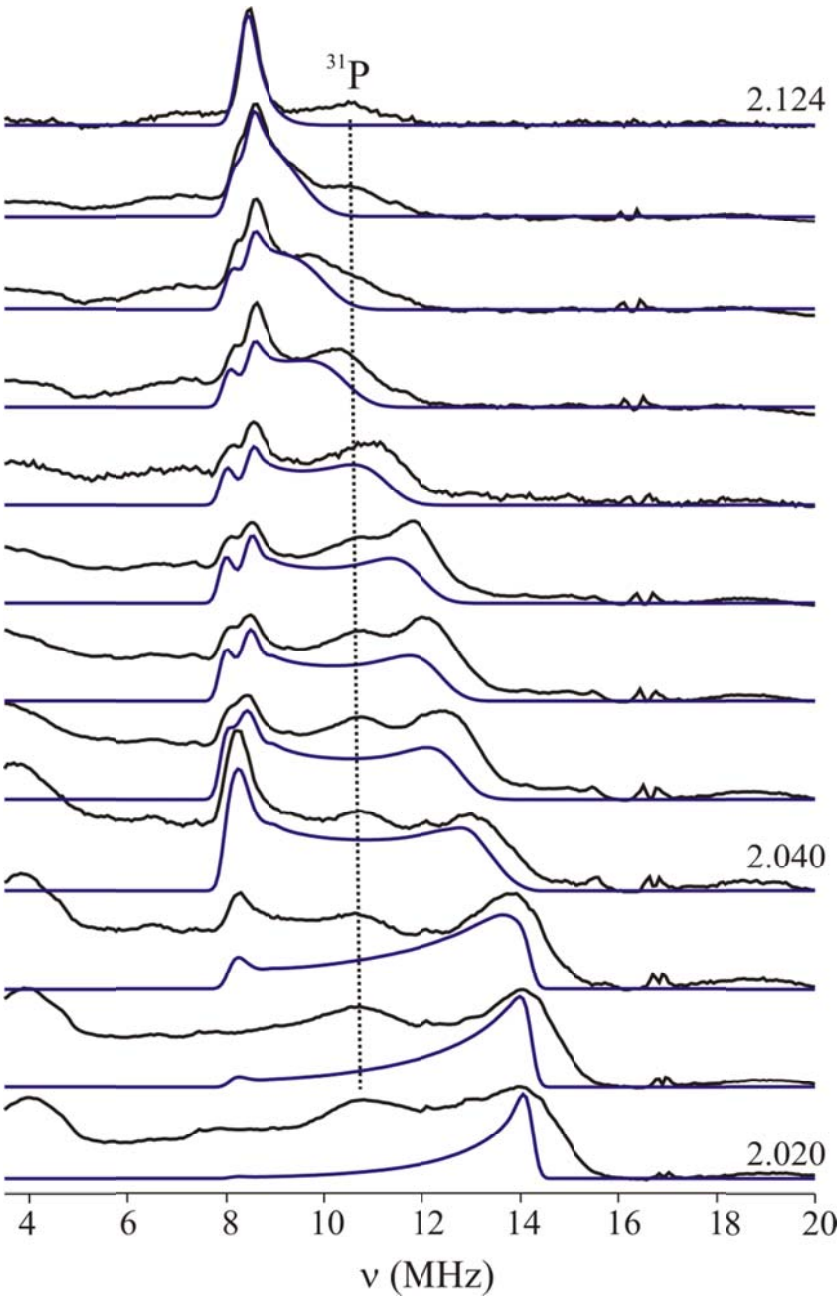

Figure A15. Davies ^{15}N pulsed ENDOR spectra from ^{15}N-**4**, 2D field-frequency pattern (black traces) with simulations (blue traces). The spectra have been simulated using a sum of two magnetically equivalent ^{15}N nuclei whose hyperfine tensors are rotated relative to **g** by $\alpha 1 = 0^o$ and $\alpha 2 = 15^o$ around the N-N vector (g_1). The dotted black line corresponds to an ENDOR response from ^{31}P nuclei in **4**. *Experimental conditions*: microwave frequency, 34.922-34.983 GHz; π = 200 ns; τ = 600 ns; t_{rf} = 30 μs; repetition rate, 20 ms; RF randomly hopped. *Simulations*. g = [2.125, 2.040, 2.020] (g_1 = z); A = [6.7, 5.6, 17.8] MHz; (φ,θ,ψ) = (90,25,90+α1:N1), (90,25,90+α2:N2); microwave frequency, 34.983 GHz; EPR linewidth, 300 MHz; ENDOR linewidth, 0.25 MHz; the ENDOR intensity from N1 and N2 have been given equal weight in the summation; the maximum simulation intensity is individually matched to the maximum ENDOR intensity at each field.

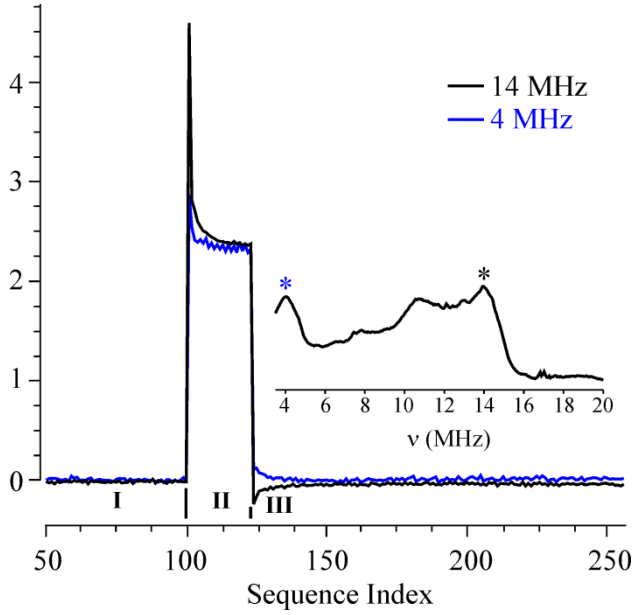

Figure A16. PESTRE spectra measured at the ν_+ (14 MHz; black) and ν_- (4 MHz; blue) frequencies from the ^{15}N ENDOR response at g_2 = 2.024 in ^{15}N-**4**. *Inset*. Davies ^{15}N ENDOR spectrum at g_2. The frequencies at which a PESTRE spectrum is acquired are denoted by stars. *Conditions*. PESTRE: microwave frequency, 34.974 GHz; π = 200 ns; τ = 600 ns; repetition rate, 25 ms; t_{rf} = 30 μs; RF frequency, 14 MHz (ν_+) and 4.0 MHz (ν_-); t_{mix} = 5 ms; ^{15}N ENDOR: π = 200 ns; τ = 600 ns; repetition rate, 20 ms; t_{rf} = 30 μs; RF frequency randomly hopped.

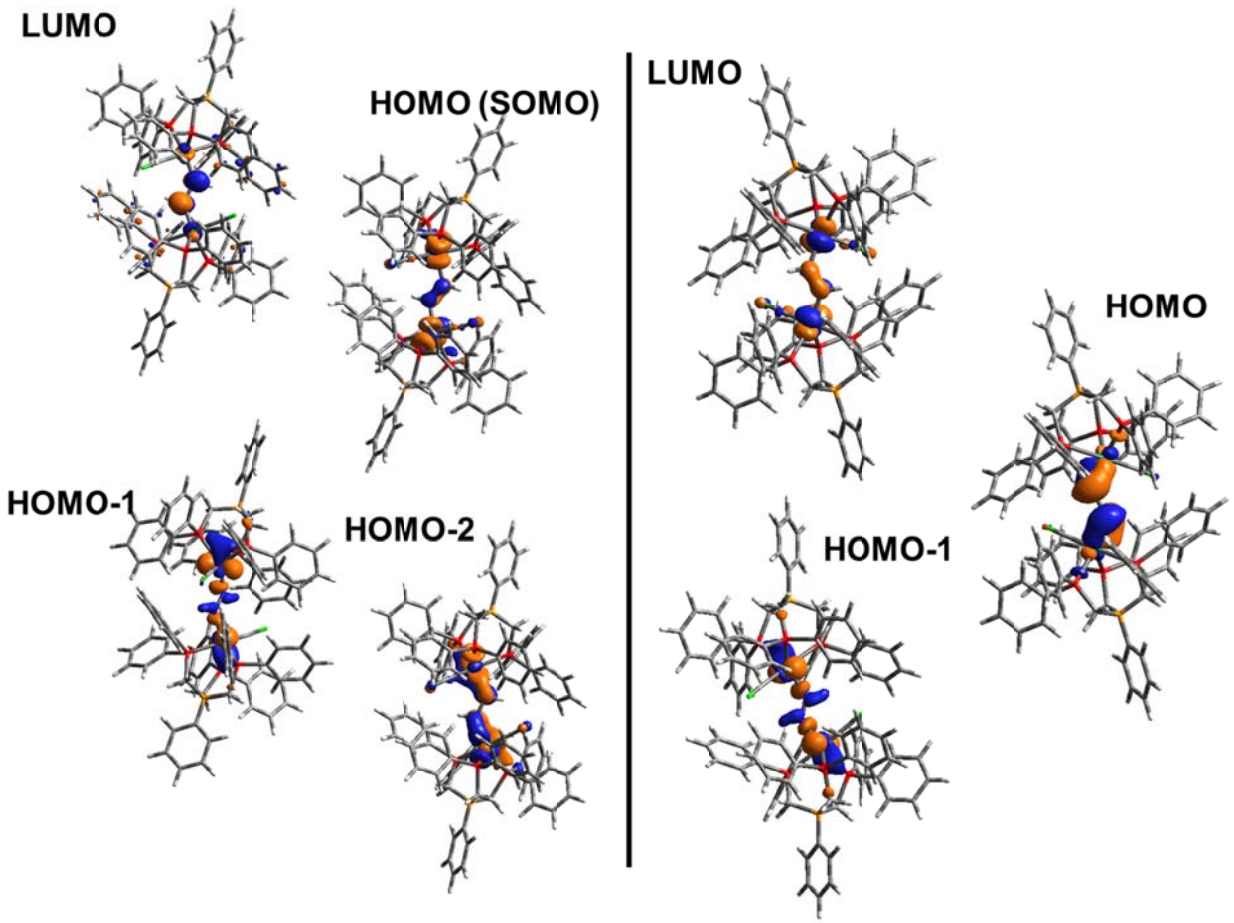

Figure A17. Isocontour plots (0.04) of the frontier orbitals of **4** (left; α spin) and **3** (right). The β orbitals for **4** were similar to the analogous α orbitals and are not shown. For the anion **4**, the energy difference between HOMO-1 and HOMO-2 is 0.67 kcal/mol (α) and 1.39 kcal/mol (β). The ordering of these orbitals is switched from that of the HOMO and HOMO-1 for **3**, in which the energy difference is 5.41 kcal/mol.

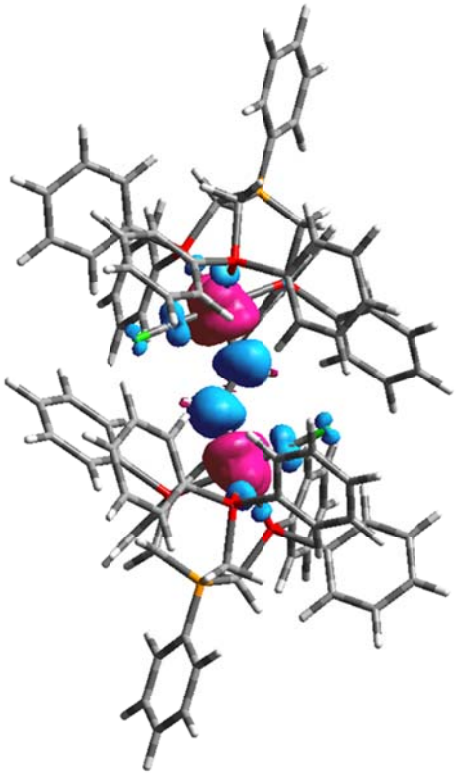

Mulliken atomic spin densities:

Fe	0.721455	Fe-NH-NH-Fe core
Fe	0.729157	
N	-0.362834	
N	-0.354171	
H	0.018239	
H	0.027385	
C	0.002566	carbonyl
O	-0.012063	
C	-0.003940	
O	-0.015531	
P	0.036846	phosphines
P	-0.013408	
P	0.034039	
P	-0.013344	
P	0.032824	
P	0.031901	

Figure A18. Isocontour plot (0.002) of the spin density of **4** with calculated densities listed. The remainder of the density (ca. 14 %) residing on the aryl rings of the ligands.

Table A1: Summary of experimental and calculated bond distances and angles for **3** and **4**. The changes in the bond distances that are experimentally observed upon reducing **3** to **4** are reproduced in the calculations, as is the overall structure of the molecule. The calculated structures are in good agreement with that obtained by XRD. The most noticeable discrepancies are the Fe-P and N-N distances, which are calculated to be ~ 0.1-0.2 Å and ~ 0.02-0.04 Å longer, respectively, than what is experimentally observed. Similar differences have been observed in related systems.[15]

Distance (Å) or Angle (^{o})	**$\{[PhBP_3Fe](CO)\}_2(\mu\text{-}N_2H_2)$, 3 (experimental)**	**$\{[PhBP_3Fe](CO)\}_2(\mu\text{-}N_2H_2)$, 3 (calculated)**	**$\{[PhBP_3Fe](CO)\}_2(\mu\text{-}N_2H_2)$, 4 (experimental)**	**$\{[PhBP_3Fe](CO)\}_2(\mu\text{-}N_2H_2)$, 4 (calculated)**
Fe1-N1 Fe2-N2 *Fe-N (ave)*	1.824(3) 1.841(3) *1.83*	1.836 1.835 *1.836*	1.876(2) 1.884(2) *1.88*	1.879 1.879 *1.879*
N1-N2	1.362(4)	1.398	1.342(3)	1.360
Fe1-P_{eq} Fe1-P_{eq} Fe2-P_{eq} Fe2-P_{eq} *Fe-P_{eq} (ave)*	2.211(1) 2.238(1) 2.216(1) 2.248(1) *2.23*	2.325 2.284 2.285 2.326 *2.31*	2.221(1) 2.237(1) 2.2069(9) 2.227(1) *2.22*	2.253 2.232 2.253 2.231 *2.42*
Fe1-P_{ax} Fe2-P_{ax} *Fe-P_{ax} (ave)*	2.325(1) 2.314(1) *2.32*	2.413 2.417 *2.425*	2.301(1) 2.2937(9) *2.30*	2.332 2.336 *2.33*
Fe1-C Fe2-C *Fe-C (ave)*	1.773(4) 1.773(4) *1.77*	1.751 1.751 *1.751*	1.750(1) 1.753(1) *1.75*	1.729 1.728 *1.729*
C-O (Fe1) C-O (Fe2) *C-O (ave)*	1.147(4) 1.150(4) *1.15*	1.159 1.159 *1.159*	1.160(4) 1.155(4) *1.16*	1.184 1.184 *1.184*
Fe1-N1-N2 Fe2-N2-N1 Fe-N-N *(ave)*	130.0(2) 131.7(2) *130.9*	133.7 133.4 *133.6*	133.1(2) 131.4(2) *132.3*	133.2 132.8 *133.0*
Fe1-N1-H1 Fe2-N2-H2 Fe-N-H (*ave*)	119(3) 122(3) *121*	119.8 120.0 *119.9*	123(2) 124(2) *124*	120.0 119.9 120.0
C-Fe-Fe-C	133	135.2	132	135.7

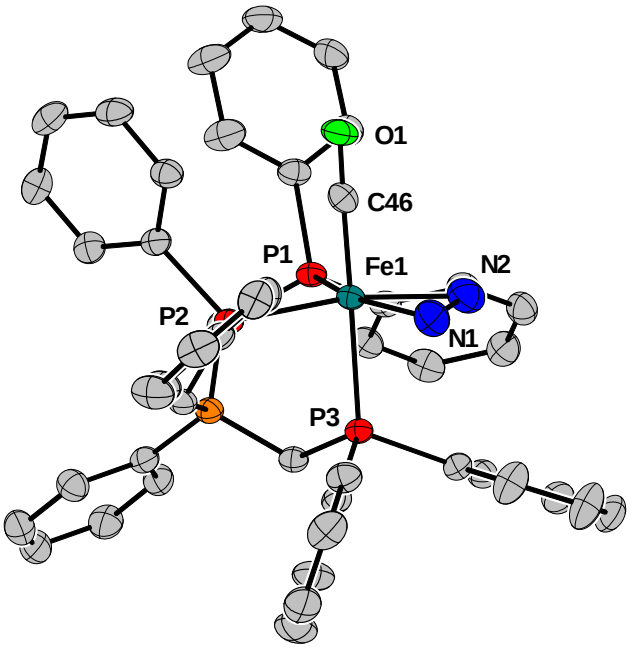

Figure A19. Displacement ellipsoid (50%) representation of **2**. Hydrogen atoms, and solvent molecules were removed for clarity.

Table A2. Select bond lengths [Å] and angles [°] for **2**.

Fe(1)-C(46)	1.758(2)	N(2)-Fe(1)-P(2)	113.23(7)
Fe(1)-N(1)	1.991(2)	C(46)-Fe(1)-P(1)	90.85(7)
Fe(1)-N(2)	2.019(2)	N(1)-Fe(1)-P(1)	113.69(7)
Fe(1)-P(2)	2.2335(6)	N(2)-Fe(1)-P(1)	153.69(7)
Fe(1)-P(1)	2.2340(6)	P(2)-Fe(1)-P(1)	92.41(2)
Fe(1)-P(3)	2.3602(6)	C(46)-Fe(1)-P(3)	179.12(7)
C(46)-O(1)	1.155(3)	N(1)-Fe(1)-P(3)	89.00(6)
N(1)-N(2)	1.383(3)	N(2)-Fe(1)-P(3)	86.77(6)
C(46)-Fe(1)-N(1)	91.85(9)	P(2)-Fe(1)-P(3)	86.83(2)
C(46)-Fe(1)-N(2)	93.75(9)	P(1)-Fe(1)-P(3)	89.00(2)
N(1)-Fe(1)-N(2)	40.33(9)	O(1)-C(46)-Fe(1)	178.5(2)
C(46)-Fe(1)-P(2)	92.31(7)	N(2)-N(1)-Fe(1)	70.94(13)
N(1)-Fe(1)-P(2)	153.49(7)	N(1)-N(2)-Fe(1)	68.73(12)

Table A3. Crystal data and structure refinement for **2**.

Identification code	d8_09026_1	
Empirical formula	C55 H53 B Fe N2 O P3	
Formula weight	917.56	
Temperature	100(2) K	
Wavelength	1.54178 Å	
Crystal system	Monoclinic	
Space group	P2(1)/c	
Unit cell dimensions	a = 22.3583(6) Å	α= 90°.
	b = 11.8150(3) Å	β= 97.956(2)°.
	c = 18.1214(6) Å	γ = 90°.
Volume	4740.9(2) $Å^3$	
Z	4	
Density (calculated)	1.286 Mg/m^3	
Absorption coefficient	3.823 mm^{-1}	
F(000)	1924	
Crystal size	0.40 x 0.22 x 0.07 mm^3	
Theta range for data collection	3.99 to 66.88°.	
Index ranges	-26<=h<=26, -14<=k<=14, -20<=l<=16	
Reflections collected	65781	
Independent reflections	8118 [R(int) = 0.0393]	
Completeness to theta = 66.88°	96.3 %	
Absorption correction	Multi-scan	
Max. and min. transmission	0.7757 and 0.3100	
Refinement method	Full-matrix least-squares on F^2	
Data / restraints / parameters	8118 / 1023 / 706	
Goodness-of-fit on F^2	1.082	
Final R indices [I>2sigma(I)]	R1 = 0.0391, wR2 = 0.1052	
R indices (all data)	R1 = 0.0436, wR2 = 0.1085	
Largest diff. peak and hole	0.968 and -0.348 $e.Å^{-3}$	

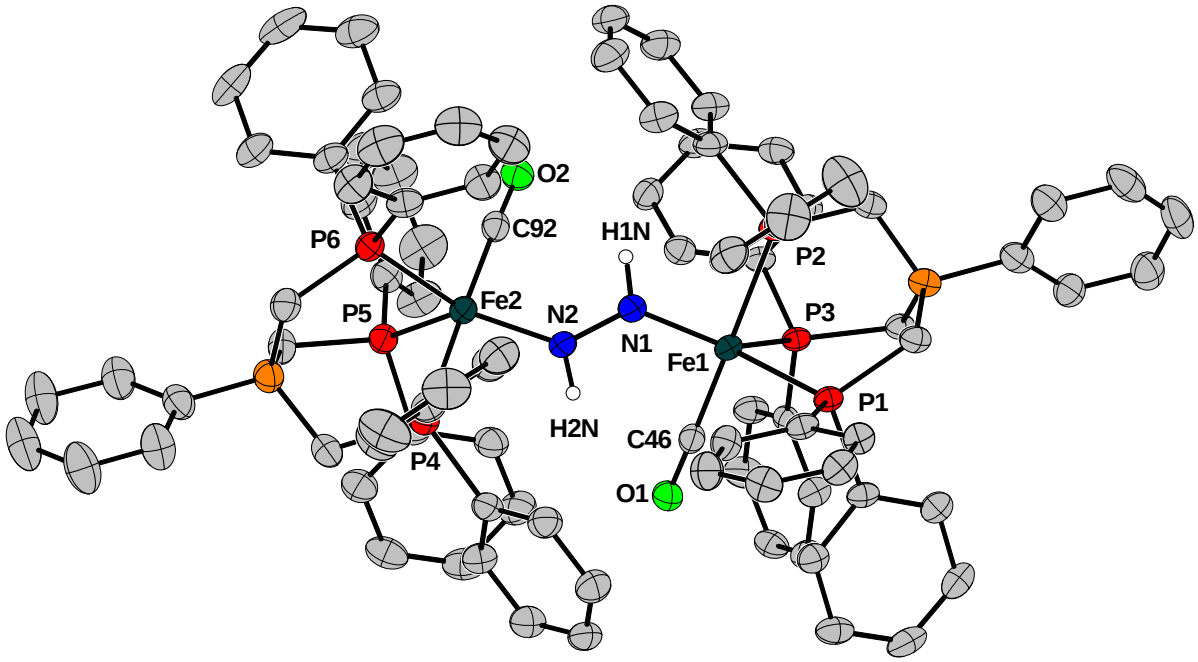

Figure A20. Displacement ellipsoid (50%) representation of **3**. Hydrogen atoms, minor components of disorder, and solvent molecules were removed for clarity.

Table A4. Select bond lengths [Å] and angles [°] for **3**.

Fe(1)-C(46)	1.773(4)	N(1)-Fe(1)-P(2)	86.12(10)
Fe(1)-N(1)	1.824(3)	P(3)-Fe(1)-P(2)	89.77(4)
Fe(1)-P(3)	2.2109(10)	P(1)-Fe(1)-P(2)	87.25(4)
Fe(1)-P(1)	2.2383(10)	N(2)-N(1)-Fe(1)	130.0(2)
Fe(1)-P(2)	2.3248(10)	N(2)-N(1)-H(1N)	110(3)
N(1)-N(2)	1.362(4)	Fe(1)-N(1)-H(1N)	119(3)
N(1)-H(1N)	0.886(18)	O(1)-C(46)-Fe(1)	175.7(3)
C(46)-O(1)	1.147(4)	C(92)-Fe(2)-N(2)	92.40(15)
Fe(2)-C(92)	1.773(4)	C(92)-Fe(2)-P(5)	91.34(12)
Fe(2)-N(2)	1.841(3)	N(2)-Fe(2)-P(5)	127.96(10)
Fe(2)-P(5)	2.2156(11)	C(92)-Fe(2)-P(6)	93.55(11)
Fe(2)-P(6)	2.2481(10)	N(2)-Fe(2)-P(6)	139.54(10)
Fe(2)-P(4)	2.3140(11)	P(5)-Fe(2)-P(6)	91.87(4)
N(2)-H(2N)	0.873(18)	C(92)-Fe(2)-P(4)	178.40(12)
C(92)-O(2)	1.150(4)	N(2)-Fe(2)-P(4)	86.09(10)
C(46)-Fe(1)-N(1)	93.15(14)	P(5)-Fe(2)-P(4)	89.17(4)
C(46)-Fe(1)-P(3)	90.60(11)	P(6)-Fe(2)-P(4)	87.94(4)
N(1)-Fe(1)-P(3)	126.62(10)	N(1)-N(2)-Fe(2)	131.7(2)
C(46)-Fe(1)-P(1)	93.37(11)	N(1)-N(2)-H(2N)	106(3)
N(1)-Fe(1)-P(1)	140.66(10)	Fe(2)-N(2)-H(2N)	122(3)
P(3)-Fe(1)-P(1)	92.05(4)	O(2)-C(92)-Fe(2)	176.5(3)
C(46)-Fe(1)-P(2)	179.26(12)		

Table A5. Crystal data and structure refinement for **3**.

Identification code	pm	
Empirical formula	C52 H48 B Fe N O P3	
Formula weight	862.48	
Temperature	100(2) K	
Wavelength	1.54178 Å	
Crystal system	Triclinic	
Space group	P-1	
Unit cell dimensions	a = 12.5497(3) Å	α= 87.989(2)°.
	b = 16.5501(4) Å	β= 76.110(2)°.
	c = 22.2784(5) Å	γ = 76.326(2)°.
Volume	4363.42(18) $Å^3$	
Z	4	
Density (calculated)	1.313 Mg/m^3	
Absorption coefficient	4.113 mm^{-1}	
F(000)	1804	
Crystal size	0.14 x 0.11 x 0.10 mm^3	
Theta range for data collection	2.04 to 65.10°.	
Index ranges	-14<=h<=14, -19<=k<=19, -26<=l<=26	
Reflections collected	85059	
Independent reflections	14565 [R(int) = 0.0639]	
Completeness to theta = 65.10°	97.8 %	
Absorption correction	Semi-empirical from equivalents	
Max. and min. transmission	0.6838 and 0.5967	
Refinement method	Full-matrix least-squares on F^2	
Data / restraints / parameters	14565 / 1506 / 1124	
Goodness-of-fit on F^2	1.072	
Final R indices [I>2sigma(I)]	R1 = 0.0556, wR2 = 0.1385	
R indices (all data)	R1 = 0.0713, wR2 = 0.1476	
Largest diff. peak and hole	1.027 and -0.670 $e.Å^{-3}$	

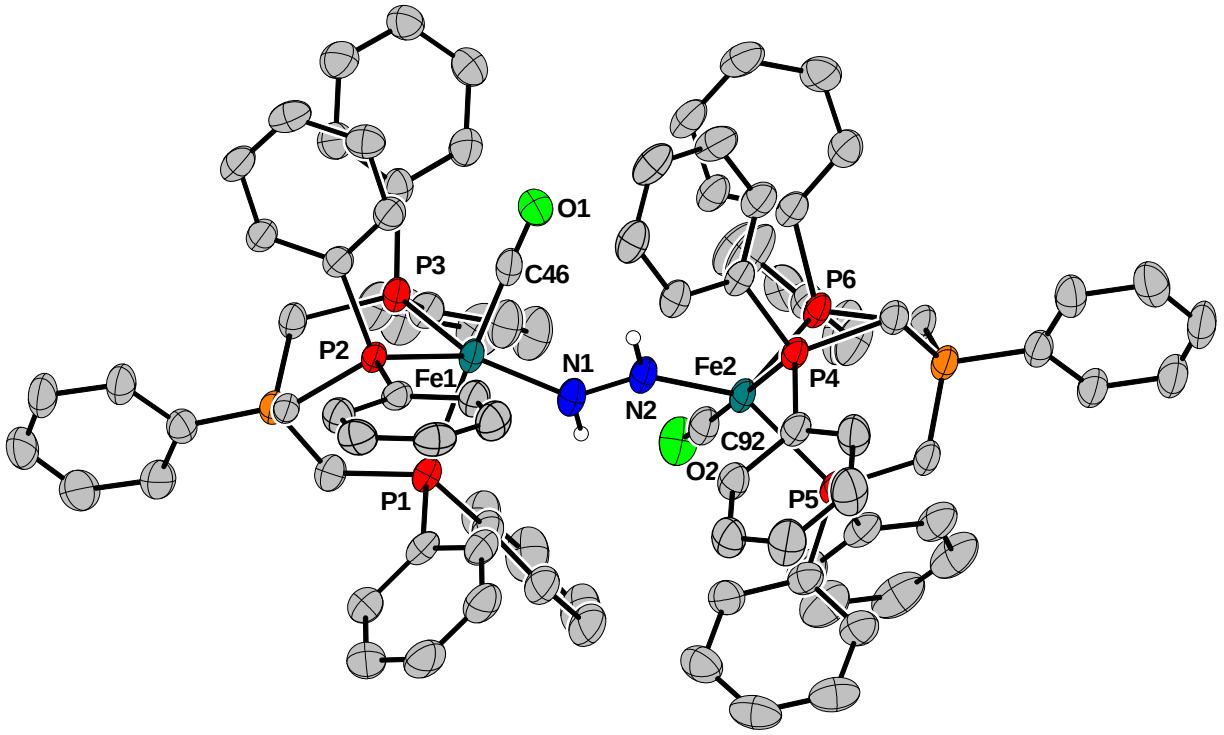

Figure A21. Displacement ellipsoid (50%) representation of **4**. Hydrogen atoms, the Na counter-cation, and solvent molecules were removed for clarity.

Table A6. Bond lengths [Å] and angles [°] for **4**.

Fe(1)-C(46)	1.750(3)	N(1)-Fe(1)-P(1)	85.27(9)
Fe(1)-N(1)	1.876(2)	P(3)-Fe(1)-P(1)	91.00(4)
Fe(1)-P(3)	2.2209(10)	P(2)-Fe(1)-P(1)	87.21(4)
Fe(1)-P(2)	2.2370(10)	N(2)-N(1)-Fe(1)	133.0(2)
Fe(1)-P(1)	2.3011(11)	N(2)-N(1)-H(1N)	103(2)
N(1)-N(2)	1.342(3)	Fe(1)-N(1)-H(1N)	123(2)
N(1)-H(1N)	0.903(19)	O(1)-C(46)-Fe(1)	176.3(2)
C(46)-O(1)	1.160(4)	C(92)-Fe(2)-N(2)	93.18(11)
Fe(2)-C(92)	1.753(3)	C(92)-Fe(2)-P(6)	89.94(10)
Fe(2)-N(2)	1.884(2)	N(2)-Fe(2)-P(6)	125.57(9)
Fe(2)-P(6)	2.2069(9)	C(92)-Fe(2)-P(5)	93.45(10)
Fe(2)-P(5)	2.2268(12)	N(2)-Fe(2)-P(5)	140.08(8)
Fe(2)-P(4)	2.2937(9)	P(6)-Fe(2)-P(5)	93.76(4)
N(2)-H(2N)	0.899(19)	C(92)-Fe(2)-P(4)	178.68(10)
C(92)-O(2)	1.155(4)	N(2)-Fe(2)-P(4)	87.33(8)
C(46)-Fe(1)-N(1)	92.77(12)	P(6)-Fe(2)-P(4)	88.77(4)
C(46)-Fe(1)-P(3)	91.08(9)	P(5)-Fe(2)-P(4)	86.93(4)
N(1)-Fe(1)-P(3)	127.21(8)	N(1)-N(2)-Fe(2)	131.42(19)
C(46)-Fe(1)-P(2)	93.64(9)	N(1)-N(2)-H(2N)	104(2)
N(1)-Fe(1)-P(2)	141.19(8)	Fe(2)-N(2)-H(2N)	124(2)
P(3)-Fe(1)-P(2)	90.89(3)	O(2)-C(92)-Fe(2)	175.9(3)
C(46)-Fe(1)-P(1)	177.75(8)		

Table A7. Crystal data and structure refinement for **4**.

Identification code	car31	
Empirical formula	C48.23 H63.12 B0.67 Fe0.67 N0.67 Na0.33 O3.10 P2	
Formula weight	815.89	
Temperature	100(1) K	
Wavelength	0.73 Å	
Crystal system	Triclinic	
Space group	P-1	
Unit cell dimensions	a = 12.380(3) Å	α= 107.95(3)°.
	b = 22.750(5) Å	β= 92.56(3)°.
	c = 24.870(5) Å	γ = 101.30(3)°.
Volume	6493(2) $Å^3$	
Z	6	
Density (calculated)	1.252 Mg/m^3	
Absorption coefficient	0.360 mm^{-1}	
F(000)	2618	
Crystal size	0.17 x 0.15 x 0.07 mm^3	
Theta range for data collection	0.87 to 25.45°.	
Index ranges	-14<=h<=14, -27<=k<=27, -30<=l<=30	
Reflections collected	219105	
Independent reflections	21306 [R(int) = 0.0852]	
Completeness to theta = 25.45°	88.7 %	
Refinement method	Full-matrix least-squares on F^2	
Data / restraints / parameters	21306 / 5305 / 1964	
Goodness-of-fit on F^2	1.024	
Final R indices [I>2sigma(I)]	R1 = 0.0500, wR2 = 0.1353	
R indices (all data)	R1 = 0.0520, wR2 = 0.1370	
Extinction coefficient	0.0063(3)	
Largest diff. peak and hole	0.557 and -0.457 e.$Å^{-3}$	

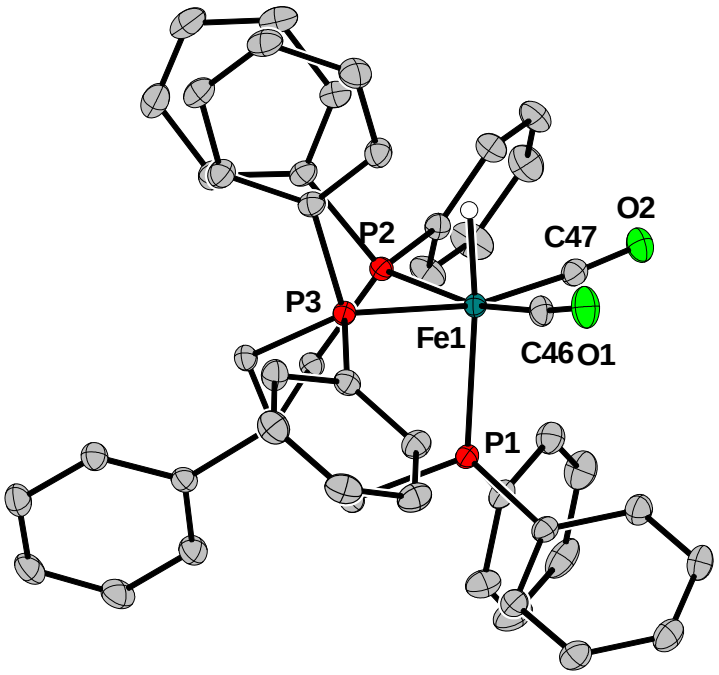

Figure A22. Displacement ellipsoid (50%) representation of **[PhBP$_3$]Fe(CO)$_2$H**. The hydride was located in the difference map, and refined. Other hydrogen atoms and solvent molecules were removed for clarity.

Table A8. Crystal data and structure refinement for **[PhBP$_3$]Fe(CO)$_2$H**.

Identification code	07141
Empirical formula	C56 H51 B Fe O2 P3
Formula weight	915.54
Temperature	100(2) K
Wavelength	0.71073 A
Crystal system, space group	Triclinic, P-1
Unit cell dimensions	a = 11.0932(11) A alpha = 88.936(2) deg.
	b = 11.1987(11) A beta = 87.070(2) deg.
	c = 20.566(2) A gamma = 64.6150(10) deg.
Volume	2305.2(4) A^3
Z, Calculated density	2, 1.319 Mg/m^3
Absorption coefficient	0.474 mm^-1
F(000)	958
Crystal size	0.35 x 0.22 x 0.10 mm
Theta range for data collection	0.99 to 29.57 deg.
Limiting indices	-15<=h<=15, -15<=k<=15, -28<=l<=28
Reflections collected / unique	61011 / 12924 [R(int) = 0.0304]
Completeness to theta = 29.57	99.8 %
Absorption correction	Semi-empirical from equivalents
Max. and min. transmission	0.9541 and 0.8516
Refinement method	Full-matrix least-squares on F^2
Data / restraints / parameters	12924 / 0 / 572
Goodness-of-fit on F^2	1.066
Final R indices [I>2sigma(I)]	R1 = 0.0320, wR2 = 0.0802
R indices (all data)	R1 = 0.0393, wR2 = 0.0887
Largest diff. peak and hole	0.539 and -0.304 e.A^-3

Table A9. Bond lengths [A] and angles [deg] for **[PhBP$_3$]Fe(CO)$_2$H**.

Fe(1)-C(46)	1.7719(14)
Fe(1)-C(47)	1.7723(14)
Fe(1)-P(2)	2.2787(4)
Fe(1)-P(1)	2.2908(4)
Fe(1)-P(3)	2.2944(4)
Fe(1)-H(57)	1.42(2)
O(1)-C(46)	1.1478(17)
O(2)-C(47)	1.1494(16)
C(46)-Fe(1)-C(47)	89.26(6)
C(46)-Fe(1)-P(2)	167.93(5)
C(47)-Fe(1)-P(2)	92.61(4)
C(46)-Fe(1)-P(1)	100.23(5)
C(47)-Fe(1)-P(1)	100.99(4)
P(2)-Fe(1)-P(1)	91.128(13)
C(46)-Fe(1)-P(3)	89.81(4)
C(47)-Fe(1)-P(3)	166.98(4)
P(2)-Fe(1)-P(3)	85.684(14)
P(1)-Fe(1)-P(3)	91.958(14)
C(46)-Fe(1)-H(57)	84.9(8)
C(47)-Fe(1)-H(57)	83.0(8)
P(2)-Fe(1)-H(57)	83.5(8)
P(1)-Fe(1)-H(57)	173.5(8)
P(3)-Fe(1)-H(57)	84.0(8)
O(1)-C(46)-Fe(1)	174.35(13)
O(2)-C(47)-Fe(1)	173.88(12)

References

[1] Davoust, C. E.; Doan, P. E.; Hoffman, B. M. *J. Magn. Reson.* **1996**, *119*, 38-44.

[2] WINEPR SimFonia, version 1.25; Bruker Biospin GmbH: Rheinstetten, Germany, 1996.

[3] (a) Kinney, R. A.; Hetterscheid, D. G. H.; Hanna, B. S.; Schrock, R. R.; Hoffman, B. M. *Inorg. Chem.* **2010**, *49*, 704. (b) P.E. Doan, J. Magn. Reson. (2010), doi:10.1016/j.jmr.2010.10.008.

[4] (a) Epel, B.; Pöppl, A.; Manikandan, P.; Vega, S.; Goldfarb, D. *J. Mag. Res.* **2001**, *148*, 388. (b) Morton, J. J. L.; Lees, N. S.; Hoffman, B. M.; Stoll, S. *J. Mag. Res.* **2008**, *191*, 315. (c) Doan, P.E., *personal communication*.

[5] Sheldrick, G. M. (1990). *Acta Cryst.* **A46**, 467.

[6] Sheldrick, G. M. (2008). *Acta Cryst.* **A64**, 112.

[7] Müller, P. *Crystallography Reviews* **2009**, *15*, 57.

[8] Spek, A. L. *PLATON A Multipurpose Crystallographic Tool*; Utrecht University: Utrecht, Holland, **2008**.

[9] W. Kabsch, *J. Appl. Cryst.* **1993**, *26*, 795.

[10] Frisch, M. J.; Trucks, G. W.; Schlegel, H. B.; Scuseria, G. E.; Robb, M. A.; Cheeseman, J. R.; Montgomery, J. A. J.; Vreven, T.; Kudin, K. N.; Burant, J. C.; Millam, J. M.; Iyengar, S. S.; Tomasi, J.; Barone, V.; Mennucci, B.; Cossi, M.; Scalmani, G.; Rega, N.; Petersson, G. A.; Nakatsuji, H.; Hada, M.; Ehara, M.; Toyota, K.; Fukuda, R.; Hasegawa, J.; Ishida, M.; Nakajima, T.; Honda, Y.; Kitao, O.; Nakai, H.; Klene, M.; Li, X.; Knox, J. E.; Hratchian, H. P.; Cross, J. B.; Adamo, C.; Jaramillo, J.; Gomperts, R.; Stratmann, R. E.; Yazyev, O.; Austin, A. J.; Cammi, R.; Pomelli, C.; Ochterski, J. W.; Ayala, P. Y.; Morokuma, K.; Voth, G. A.; Salvador, P.; Dannenberg, J. J.; Zakrzewski, V. G.; Dapprich, S.; Daniels, A. D.; Strain, M. C.; Farkas, O.; Malick, D. K.; Rabuck, A. D.; Raghavachari, K.; Foresman, J. B.; Ortiz, J. V.; Cui, Q.; Baboul, A. G.; Clifford, S.; Cioslowski, J.; Stefanov, B. B.; Liu, G.; Liashenko, A.; Piskorz, P.; Komaromi, I.; Martin, R. L.; Fox, D. J.; Keith, T.; Al-Laham, M. A.; Peng, C. Y.; Nanayakkara, A.; Challacombe, M.; Gill, P. M. W.; Johnson, B.; Chen, W.; Wong, M. W.; Gonzalez, C.; Pople, J. A. Gaussian03, Rev. C02; Gaussian, Inc.: Pittsburgh PA, 2004.

[11] GaussView, Version 4.1; Roy Dennington II, Todd Keith and John Millam, Semichem, Inc., Shawnee Mission, KS, 2007.

[12] Saouma, C. T.; Müller, P.; Peters, J. C. *J. Am. Chem. Soc.* **2009**, *131*, 10358.

[13] Saouma, C. T.; Peters, J. C. *manuscript in preparation*. Treatment of $[PhBP_3]FeCl$ with two equivalents of Na/Hg under a CO atmosphere generates $[PhBP_3]Fe(CO)_2Na(THF)_6$.

[14] Schrock, R. R.; Liu, A. H.; O'Regan, M. B.; Finch, W. C.; Payack, J. F. *Inorg. Chem.* **1988**, *27*, 3574.

[15] (a) Jenkins, D. M.; Peters, J. C. *J. Am. Chem. Soc.* **2005**, *127*, 7148. (b) Macbeth, C. E.; Thomas, J. C.; Betley, T. A.; Peters, J. C. *Inorg. Chem.* **2004**, *43*, 4645.